Check for updates

JGR Solid Earth

RESEARCH ARTICLE
10.1029/2026JB033855

Weakening Processes in Carbonate-Hosted Faults: Phyllosilicate Microlayers and Injections Along the Mattinata Fault (Southern Italy)

Rachele Calvanelli[1], Luca Aldega[1], Andrea Billi[2], Andrea Cavallo[3], Manuel Curzi[1], Marco Mercuri[1], Michele Morsilli[4], Alessio Pontesilli[5], Cecilia Viti[6], and Eugenio Carminati[1]

[1]Dipartimento di Scienze della Terra, Sapienza Università di Roma, Rome, Italy, [2]Consiglio Nazionale delle Ricerche, IGAG, Rome, Italy, [3]CERTEMA Ricerca e Innovazione, Grosseto, Italy, [4]Dipartimento di Fisica e Scienze della Terra, Università di Ferrara, Ferrara, Italy, [5]Istituto Nazionale di Geofisica e Vulcanologia, Rome, Italy, [6]Dipartimento di Scienze Fisiche, della Terra e dell'Ambiente, Università di Siena, Siena, Italy

Abstract Micrometric phyllosilicate films along fault slip surfaces (SSs) can drastically reduce friction, yet they are unexpected in clay-poor carbonate platforms. We inquire how a major carbonate-hosted, seismogenic strike-slip fault can develop weak slip interfaces and undergo dynamic weakening despite an intrinsically strong host rock. Along the Mattinata Fault (Gargano Promontory, southern Italy), we integrate structural mapping and drone-based virtual outcrops with microstructural, mineralogical, and geochemical analyses (optical microscopy, SEM/FESEM-EDS, EPMA, and XRD). We document micrometric illite- and kaolinite-rich microlayers (locally up to ∼15 μm thick) localized on some SSs, together with ultracataclasites and phyllosilicate-filled injection veins that emanate from these surfaces into otherwise nearly pure calcite host rocks. Microtextures, vein geometries, and mineral assemblages suggest that clay minerals were derived from outside the carbonate host rock and introduced by transient fluid pressurization during coseismic slip, reflecting episodic open-system behavior of the fault zone. Because high-velocity experiments show that even minimal amounts of phyllosilicates concentrated in thin films can promote strong dynamic weakening, our observations provide a field-based mechanism for rapid weakening and slip localization in carbonate-hosted foreland faults. More broadly, we show that seismogenic faults in carbonate may be (unexpectedly and cryptically) clay-bearing, with important consequences for rupture propagation and for laboratory and numerical models that commonly assume closed, clay-free systems.

Plain Language Summary High stress accumulation and large stress drop can occur on faults cutting strong rocks such as carbonate platforms. These faults are often assumed to be strong, yet many show evidence of abrupt weakening during seismic slip. We investigate this paradox at the Mattinata Fault in southern Italy, a strike-slip structure capable of magnitude 6–7 earthquakes and hosted in nearly pure carbonates within a foreland domain. Through detailed field surveys, 3D virtual outcrops, and laboratory-based microscopic, chemical, and mineralogical analyses, we identify extremely thin films of clay minerals along fault slip surfaces (SSs) and associated injection veins. We infer that these clay-rich microlayers formed when transient pressurized fluids during past earthquakes injected externally sourced clay into the fault zone. Even where the host rocks contain negligible clay minerals, such processes can localize weak minerals into ultra-thin coatings where slip is concentrated. Laboratory experiments indicate that small clay fractions, when focused along SSs, can markedly reduce friction at earthquake slip rates. Our results show that carbonate-hosted faults can become dynamically weak through open-system inputs of clay minerals driven by coseismic fluid-pressure pulses. This implies that models of rupture in carbonates should incorporate clay transport and transient fluid pressurization to capture dynamic weakening.

Key Points:

- A major strike slip fault in pure carbonate rocks hosts unexpected clay minerals microlayers on its slip surfaces
- External fluids inject clay minerals into the fault zone forming ultra-thin weak coatings that contribute to seismic rupture propagation
- Even small amounts of clay minerals localized in these coatings can promote dynamic weakening

Supporting Information:

Supporting Information may be found in the online version of this article.

Correspondence to:

R. Calvanelli and A. Billi,
rachele.calvanelli@uniroma1.it;
andrea.billi@cnr.it

Citation:

Calvanelli, R., Aldega, L., Billi, A., Cavallo, A., Curzi, M., Mercuri, M., et al. (2026). Weakening processes in carbonate-hosted faults: Phyllosilicate microlayers and injections along the Mattinata fault (Southern Italy). *Journal of Geophysical Research: Solid Earth*, *131*, e2026JB033855. https://doi.org/10.1029/2026JB033855

Received 16 JAN 2026
Accepted 4 MAY 2026

Author Contributions:

Conceptualization: Rachele Calvanelli, Luca Aldega, Andrea Billi, Manuel Curzi, Marco Mercuri, Eugenio Carminati
Data curation: Rachele Calvanelli, Luca Aldega, Andrea Billi, Andrea Cavallo, Manuel Curzi, Marco Mercuri
Formal analysis: Rachele Calvanelli, Luca Aldega, Andrea Billi, Andrea Cavallo, Manuel Curzi, Marco Mercuri, Michele Morsilli, Alessio Pontesilli, Cecilia Viti, Eugenio Carminati
Funding acquisition: Eugenio Carminati

© 2026. The Author(s).
This is an open access article under the terms of the Creative Commons Attribution License, which permits use, distribution and reproduction in any medium, provided the original work is properly cited.

1. Introduction

The mechanics of fault slip and earthquake nucleation remain central questions in seismology and structural geology. A fundamental control on these processes is the frictional behavior of fault zone rocks, which governs fault strength and the conditions under which slip initiates and propagates (Scholz, 1998; Sibson, 1977). During earthquakes, however, rupture propagation and slip acceleration are controlled by dynamic weakening processes that operate at seismic slip rates, including flash and thermal heating, thermal pressurization of pore fluids, grain-

21699356, 2026, 5, Downloaded from https://agupubs.onlinelibrary.wiley.com/doi/10.1029/2026JB033855 by Andrea Billi - University Di Roma La Sapienza , Wiley Online Library on [14/05/2026]. See the Terms and Conditions (https://onlinelibrary.wiley.com/terms-and-conditions) on Wiley Online Library for rules of use; OA articles are governed by the applicable Creative Commons License

Investigation: Rachele Calvanelli, Luca Aldega, Andrea Billi, Andrea Cavallo, Manuel Curzi, Marco Mercuri, Michele Morsilli, Alessio Pontesilli, Cecilia Viti, Eugenio Carminati
Methodology: Rachele Calvanelli, Luca Aldega, Andrea Billi, Andrea Cavallo, Manuel Curzi, Marco Mercuri, Alessio Pontesilli, Cecilia Viti
Project administration: Eugenio Carminati
Supervision: Eugenio Carminati
Validation: Rachele Calvanelli, Luca Aldega
Writing – original draft: Rachele Calvanelli, Luca Aldega, Andrea Billi, Manuel Curzi, Marco Mercuri, Michele Morsilli, Eugenio Carminati
Writing – review & editing: Rachele Calvanelli, Luca Aldega, Andrea Billi, Andrea Cavallo, Manuel Curzi, Marco Mercuri, Michele Morsilli, Alessio Pontesilli, Cecilia Viti, Eugenio Carminati

size reduction, gouge lubrication, or even frictional melting and melt lubrication (e.g., Di Toro et al., 2011; Rice, 2006, and references therein).

Within this broader framework, growing experimental and field evidence shows that even minor volumes of phyllosilicates can markedly reduce frictional strength (e.g., Ruggieri et al., 2021) or promote dynamic weakening at seismic slip rates (e.g., Bullock et al., 2015; Smeraglia, Billi, et al., 2017, Smeraglia, Bettucci, et al., 2017). Phyllosilicate-assisted weakening has been documented in a variety of tectonic settings, including subduction zones (Ikari et al., 2009; Kirkpatrick et al., 2025; Vannucchi et al., 2008), extensional detachments (Collettini et al., 2009; Viti & Collettini, 2009), and strike-slip faults (Carpenter et al., 2011; Faulkner et al., 2003; Moore & Lockner, 2004). Consequently, constraining both the distribution and abundance of phyllosilicates along faults as well as the related mechanisms of emplacement is essential to understand their mechanical effects and evaluate their implications for fault slip behavior.

Phyllosilicate-rich layers along fault surfaces are most commonly reported where clay minerals are readily available—either because the host rock is intrinsically clay-bearing (e.g., marly limestones; Tesei et al., 2013; Bullock et al., 2014) or because fault architecture juxtaposes carbonate units against clay-rich formations, such as syn-tectonic siliciclastic turbidites in fold-and-thrust belts (Coppola et al., 2021; Smeraglia et al., 2016). In these settings, the high availability of phyllosilicates favors their incorporation into the fault core, impacting fault slip behavior.

By contrast, clay minerals are generally scarce in nearly pure platform carbonates of foreland domains, where thick carbonate successions are not overlain by an orogenic turbiditic cover. Accordingly, phyllosilicates are expected to be absent or less frequent and less abundant along SSs in these settings, given the limited internal supply within the sedimentary succession. Nevertheless, in carbonate-dominated systems it remains essential to quantify the abundance and constrain the provenance of any fault-related phyllosilicates, because even minor amounts can promote coseismic dynamic weakening (Bullock et al., 2015; Smeraglia, Billi, et al., 2017, Smeraglia, Bettucci, et al., 2017).

The Apulian foreland of southern Italy serves as a natural laboratory to investigate such a situation. This region is characterized by a ∼5 km thick Mesozoic–Cenozoic carbonate sequences (mostly platform environment) cut by large-scale strike-slip faults, notably the Mattinata Fault (MF) system in the Gargano Promontory, which has sourced both historical and recent instrumental seismicity up to Mw 6–7 (Figures 1a–1c) (Del Gaudio et al., 2007; Miccolis et al., 2021). Contrary to other seismically active areas of Italy, mainly in the axial sector of the Apennines fold-thrust belt, this foreland domain lacks clay-rich turbiditic deposits.

In this study, we integrate field observations with microstructural, mineralogical and chemical data from well-exposed segments of the MF to address two main questions: (a) can a foreland fault hosted by nearly pure platform carbonates develop clay-rich slip interfaces, or other conditions potentially conducive to coseismic slip localization and dynamic weakening, despite the scarcity of phyllosilicates in the host rocks? and (b) if so, what are the sources of these weak minerals, and by which transport and emplacement processes are they delivered to and concentrated along slip surfaces (SSs) in an otherwise clay-poor system?

We document ultracataclasites and unexpected, micrometer-scale phyllosilicate layers localized along carbonate-hosted SSs and evaluate their origin by combining X-ray diffraction (XRD), scanning and field-emission electron microscopy (SEM/FESEM), and electron probe microanalysis (EPMA). We specifically test the contribution of external clay mineral sources—spotty *terra rossa* pockets and rare clay-rich beds in the local sedimentary succession—and hypothesize the role of transient, pressurized fluid pulses during slip in concentrating weak minerals into ultra-thin, potentially low-friction microlayers.

These observations broaden current views of rupture behavior in carbonate-hosted faults by highlighting that weak, phyllosilicate-rich material can be introduced and concentrated along slip zones (SZ) even where the surrounding stratigraphy is clay-poor. By demonstrating that a major seismogenic fault cutting nearly pure platform carbonates can nonetheless accumulate phyllosilicates along its SSs, our work supports an open-system perspective on fault-zone evolution and weakening in clay-poor foreland domains. Our results are therefore directly relevant to interpret natural carbonate-hosted seismogenic faults and to design numerical and laboratory friction experiments that aim to reproduce their mechanical behavior.

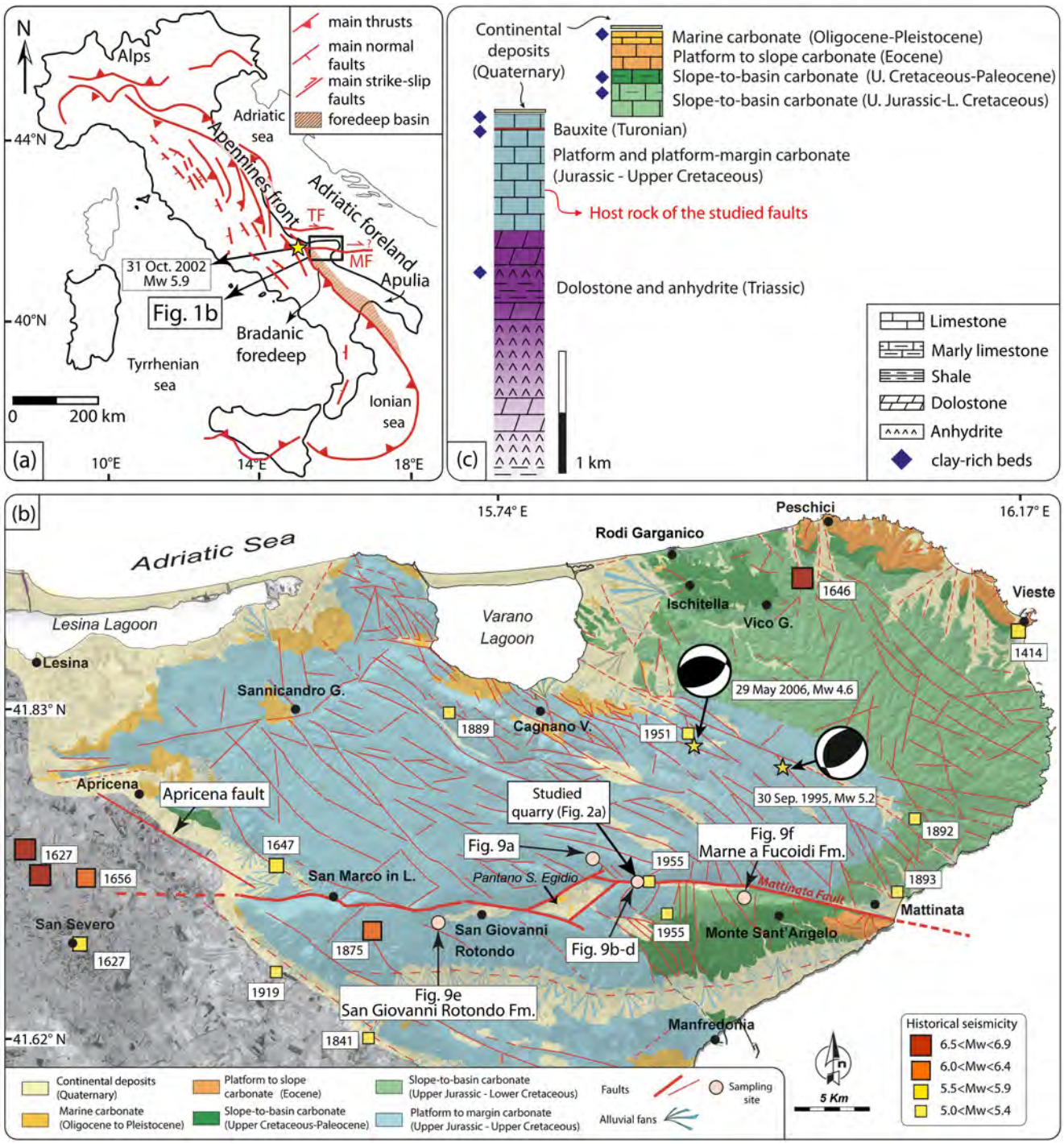

Figure 1. (a) Simplified structural map of Italy showing major (active) thrusts and normal faults of the Apennine fold-and-thrust belt. The Gargano Promontory is located in the Adriatic (locally Apulian) foreland, east of the Apennines fold-and-thrust belt and foredeep. (b) Simplified geological map of the Gargano Promontory (modified after Morsilli, 2016) showing faults (red lines) and main lithostratigraphic units reported in panel (c). Pink circles mark the sampling sites. Epicentral areas of historical earthquakes (Mw ≥ 5) from the Parametric Catalog of Italian Earthquakes (CPTI11, https://ingvterremoti.com/) are represented with colored squares. Locations of instrumental earthquake epicenters and their corresponding focal mechanisms are reported with yellow stars and are retrieved from the Centroid-Moment Tensor catalog of Harvard University. (c) Simplified stratigraphic log showing the main lithostratigraphic units of the Gargano Promontory. Blue diamonds highlight the presence of some clay-rich beds within the almost pure carbonate succession. Note that the fault exposures analyzed in this paper occur in the Upper Jurassic-Lower Cretaceous platform carbonate of the Monte Spigno Fm.

21699356, 2026, 5, Downloaded from https://agupubs.onlinelibrary.wiley.com/doi/10.1029/2026JB033855 by Andrea Billi - University Di Roma La Sapienza , Wiley Online Library on [14/05/2026]. See the Terms and Conditions (https://onlinelibrary.wiley.com/terms-and-conditions) on Wiley Online Library for rules of use; OA articles are governed by the applicable Creative Commons License

2. Geological Setting

2.1. Tectonic Framework of the Southern Apennines

The Southern Apennines form a NW–SE-trending fold-and-thrust belt developed during the Neogene–Quaternary convergence between the Adriatic and European plates. This evolution was driven by SW-directed subduction and NE-retreat of the Adriatic slab (Carminati et al., 2012; Malinverno & Ryan, 1986). Since the Miocene, slab rollback has promoted eastward migration of the compressional front and crustal stretching of the belt's interior, leading to the opening of the Tyrrhenian back-arc basin (Malinverno & Ryan, 1986). As a result, both compressional and extensional tectonics coexist in the region (Vezzani et al., 2010).

The Adriatic foreland, to the east of the Apennine belt (Figure 1a), includes the Apulian Carbonate Platform (ACP), a Mesozoic–Cenozoic carbonate domain extending from southeastern Italy into the Adriatic and Ionian offshore (Argnani et al., 2009; Bosellini et al., 1999). East of the Bradanic foredeep (Patacca & Scandone, 2004a), the ACP is widely exposed across Apulia, forming a relatively stable and elevated foreland block. The Gargano Promontory, part of the Apulian foreland, shows more intense deformation, including folding and faulting along structures such as the E–W-trending MF system (Argnani et al., 1993; Bertotti et al., 1999; Brankman & Aydin, 2004; Chilovi et al., 2000; Funiciello et al., 1988).

Unlike other foreland sectors, the Gargano Promontory underwent significant uplift since at least the Late Miocene, attributed to both Dinaric and Apenninic tectonics (Argnani et al., 1993; Bertotti et al., 1999; Brankman & Aydin, 2004; Funiciello et al., 1988). More recent uplift phases may reflect the subduction of the thick Adriatic lithosphere south of the Tremiti Fault (TF) system, with consequent decrease of slab penetration (Carminati & Doglioni, 2005; Doglioni et al., 1994). Within this context, the MF and Tremiti Fault (TF, Figure 1a) may represent major crustal-scale strike-slip systems that have accommodated the differential retreat of the Apennines subduction system, via deformation across the Apulian foreland (Doglioni et al., 1994; Petricca et al., 2013).

2.2. The Mattinata Fault

The MF across the Gargano Promontory is a crustal-scale, first-order strike-slip fault. The fault strikes E-W and extends for ∼150 km, with ∼50 km onshore and ∼100 km offshore (Argnani et al., 1993, 2009; Billi et al., 2007; Nicolai & Gambini, 2007; Tondi et al., 2005). The MF bounds toward the south a WNW–ESE-trending anticline segmented by multiple fault systems across the entire Gargano Promontory (Argnani et al., 2009; Billi et al., 2007; Funiciello et al., 1988).

The MF zone is up to ∼300 m wide, with a well-defined fault core and damage zone, and clear surface expression (Salvini et al., 1999). The best exposure of the MF is located between the villages of San Giovanni Rotondo and Monte Sant'Angelo (Figure 1b), where it cuts Upper Jurassic-Lower Cretaceous platform margin carbonates of the Monte Spigno Fm.

The MF kinematics is complex and still debated. While some authors interpreted it as left-lateral (Billi et al., 2007; Billi & Salvini, 2003; Brankman & Aydin, 2004; Funiciello et al., 1988; Salvini et al., 1999), others argued for right-lateral displacement (Di Bucci et al., 2006; Doglioni et al., 1994). A multiphase evolution with both senses of motion was also proposed (Chilovi et al., 2000; Tondi et al., 2005). Other studies emphasized its transpressional kinematics (Nicolai & Gambini, 2007) or the inheritance of Mesozoic extensional faults (Argnani et al., 1993, 2009). The timing of faulting onset remains debated, with estimates ranging from Oligocene–Miocene (Argnani et al., 2009) to Late Miocene (Billi et al., 2007).

2.3. Seismic Setting

The Gargano Promontory forms an uplifted sector of the Apulian foreland, bounded and dissected by a long-lived, predominantly E–W–striking strike-slip system and subordinate normal faults, among which the MF and Apricena Fault are the most prominent seismogenic structures (e.g., Argnani et al., 2009; Billi et al., 2007; Tinti et al., 1995). This structural setting produced several damaging historical earthquakes, some of which also generated tsunamis in the southern Adriatic Sea (Fracassi et al., 2012; Tinti & Piatanesi, 1996).

Historical catalogs and recent reassessments document a sequence of medium-to-large earthquakes affecting the Gargano area (Figure 1b) since at least the thirteenth century, culminating in a destructive seventeenth-century seismicity (Camassi et al., 2008; Del Gaudio et al., 2007; Miccolis et al., 2021). The largest known

21699356, 2026, 5, Downloaded from https://agupubs.onlinelibrary.wiley.com/doi/10.1029/2026JB033855 by Andrea Billi - University Di Roma La Sapienza , Wiley Online Library on [14/05/2026]. See the Terms and Conditions (https://onlinelibrary.wiley.com/terms-and-conditions) on Wiley Online Library for rules of use; OA articles are governed by the applicable Creative Commons License

21699356, 2026, 5, Downloaded from https://agupubs.onlinelibrary.wiley.com/doi/10.1029/2026JB033855 by Andrea Billi - University Di Roma La Sapienza , Wiley Online Library on [14/05/2026]. See the Terms and Conditions (https://onlinelibrary.wiley.com/terms-and-conditions) on Wiley Online Library for rules of use; OA articles are governed by the applicable Creative Commons License

earthquake is the 1627 earthquake (Mw ≈ 6.7), which devastated large portions of the promontory and adjacent areas, causing several thousand casualties and triggering a damaging tsunami along the Apulian and Dalmatian coasts (Patacca & Scandone, 2004b; Tinti & Piatanesi, 1996).

Subsequent damaging earthquakes (Figure 1b) include the 31 May 1646 event (I ≈ X, Mw ≈ 6.2), which produced widespread destruction across northern Gargano and is now recognized as part of a clustered seventeenth-century activation of different MF segments (Camassi et al., 2008). Other earthquakes occurred in 1889 and 1893 (Mw ≈ 5.2–5.4), with the 10 August 1893 earthquake reaching intensity IX–X in the Mattinata area and commonly associated with the MF (Fracassi et al., 2012). Instrumental catalogs show additional moderate events, notably the 1995 (Mw 5.2) and 2006 (Mw 4.6) earthquakes, confirming that the entire upper crust beneath Gargano remains seismically active (Camassi et al., 2008; Miccolis et al., 2021).

Recent local-network observations (2013–2018) further reveal distributed microseismicity down to ∼40 km depth, with focal mechanisms indicating coexistence of thrust and dextral strike-slip faulting consistent with reactivation of inherited E–W striking faults within the Apulian foreland (Ferreri et al., 2025; Filippucci et al., 2021; Miccolis et al., 2021). Regional seismotectonic models suggest that these E–W right-lateral structures continue westward beneath the Apenninic front (Figure 1a; Argnani et al., 2009; Di Bucci et al., 2006; Milano et al., 2005). In this framework, the Mw 5.8–5.9 October–November 2002 Molise earthquake sequence (to the west of the MF area; Figure 1a), whose mainshocks produced damages and deaths, has been interpreted as a rupture of a west–east strike-slip fault segment at the top of the Apulian Platform, possibly representing the westward continuation of the MF beneath the Southern Apennines (Chiarabba et al., 2014; Di Bucci & Mazzoli, 2003; Vallée & Di Luccio, 2005).

The maximum seismic potential of the MF is considered to be Mw 6.5/7.0, based on empirical scaling relationships between fault length and earthquake magnitude (Trippetta et al., 2019). For this reason, understanding lithological and rheological properties of the MF SS is scientifically and societally relevant.

3. Methods and Nomenclature

We investigated the freshest and best-preserved SSs exposed along the walls of the recently active San Simeone quarry, which intersects the MF near Monte Sant'Angelo (Figures 1b and 2a). Field surveys and meso-structural analyses were integrated with high-resolution Structure-from-Motion (SfM) multi-view stereophotogrammetry acquired using a drone. This approach enabled the construction of an aerial orthomosaic and a Virtual Outcrop Model (VOM; Figures 2a and 2b). Strategic sampling was performed within the quarry and in the surrounding area (Figure 1b; Table S1 in Supporting Information S1). We collected carbonate fault rocks together with their host rocks. Selected fault rock samples were cut orthogonal to the SS and parallel to the slip direction. Related thin-sections, small slabs or powders were analyzed using optical microscopy, Scanning Electron Microscopy (SEM), Field-Emission Scanning Electron Microscopy (FESEM) with energy-dispersive spectroscopy (EDS), Electron Probe Microanalysis (EPMA), and XRD (Table S1 in Supporting Information S1).

Unexpected microlayers or nanolayers of phyllosilicates were identified along some SSs and associated fractures (see below). To constrain the origin of these phyllosilicates within an otherwise clay-poor carbonate host, we carried out additional targeted sampling and analyses. We collected phyllosilicate-rich rocks and residual soils (*terra rossa*) from the vicinity of the studied faults (see Figure 1b for sampling locations). These samples were prepared and analyzed by XRD.

We use the term host rock or near host rock to refer to carbonate rocks adjacent to the fault (within centimeters) and not affected by cataclasis. However, because the investigated quarries are located within the MF zone—specifically within the fault core and damage zone (Salvini et al., 1999)—this host rock should not be considered strictly undeformed or pristine. We therefore use the term remote host rock to indicate carbonate rocks located outside the fault zone (hundreds of meters at least from the MF).

Additional methodological details and data are provided in the (Figures S1–S13 and Tables S1–S2 in Supporting Information S1).

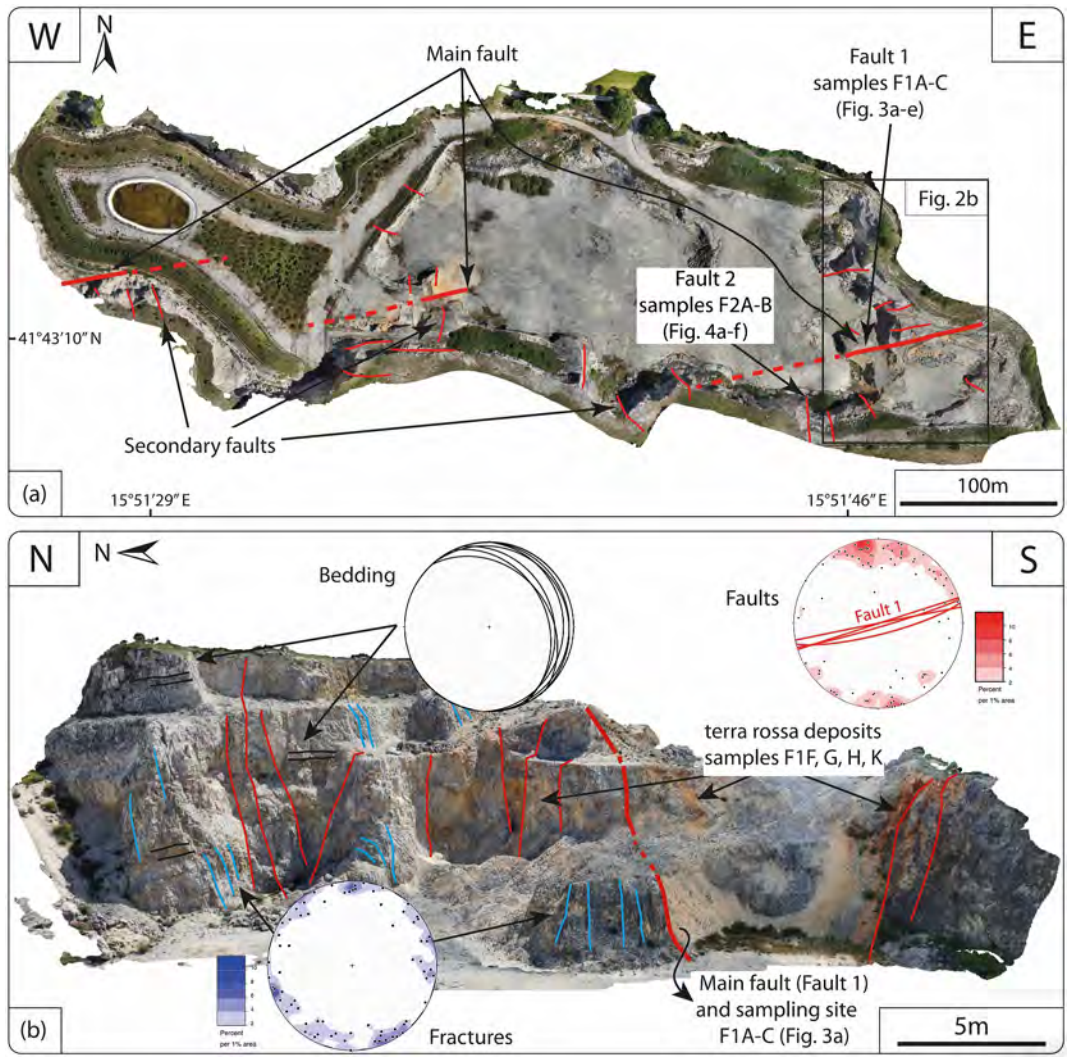

Figure 2. (a) Aerial orthomosaic of the studied quarry, highlighting fault sets and sampling location. The main fault set, parallel to the regional trend of the Mattinata Fault, is marked with thick red lines. (b) Virtual outcrop model of the eastern quarry wall (see panel a), where the main fault set is well exposed. Faults (red lines), fractures-including joints and shear fractures (blue lines), and bedding (black lines) are shown. Schmidt nets (lower hemisphere projections) illustrate the orientations of bedding, fractures, and faults. Faults and fractures are represented as poles to planes (contoured using the 1% area method), while Fault 1 and bedding are shown as a cyclograph.

4. Data and Results

4.1. Analysis of Faults

4.1.1. Field Structural Analyses and Virtual Outcrops

In the analyzed quarry (Figures 1b and 2a), the platform carbonate of the Monte Spigno Fm. is exposed. Field observations and VOM analysis reveal a dense fracture network of joints and faults. Bedding is locally preserved although partly masked by fractures, and dips gently (5°–10°) toward the E–NE (Figure 2b).

Four main fault sets with distinct orientations cut the quarry walls (Figures 2a and 2b). The dominant ENE–WSW striking set aligns with the regional MF trend and features fault cores ranging from a few tens of centimeters to ~1 m in thickness (Figures 2b and 3a). The main ENE–WSW faults are steeply dipping (65°–87°), either to the SSE- or to NNW, and exhibit strike-slip kinematics. Subordinate fault sets strike N–S, NE–SW, and NW–SE and are characterized by thinner fault cores (centimeter-scale; Figures 2b and 4a).

21699356, 2026, 5, Downloaded from https://agupubs.onlinelibrary.wiley.com/doi/10.1029/2026JB033855 by Andrea Billi - University Di Roma La Sapienza , Wiley Online Library on [14/05/2026]. See the Terms and Conditions (https://onlinelibrary.wiley.com/terms-and-conditions) on Wiley Online Library for rules of use; OA articles are governed by the applicable Creative Commons License

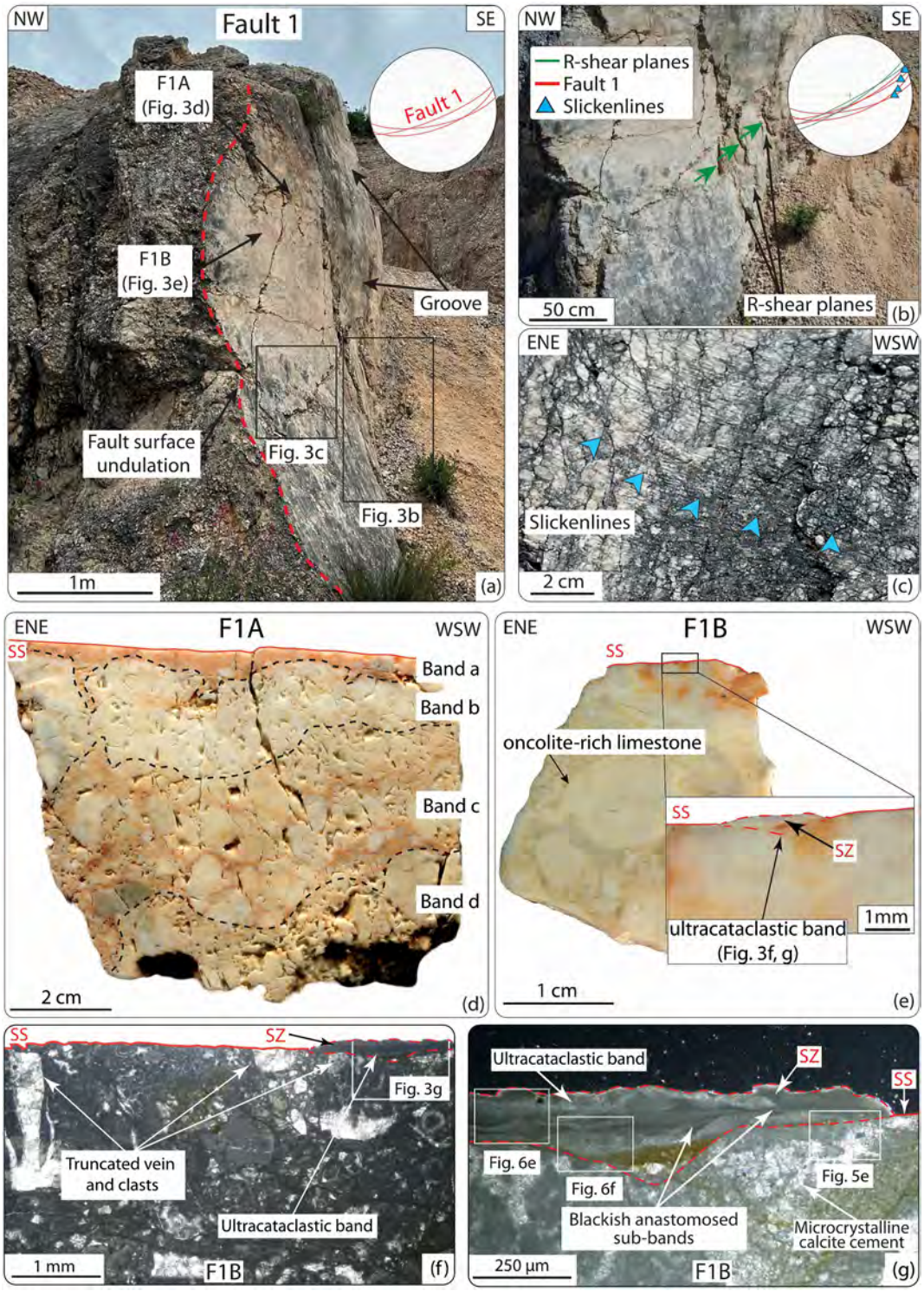

Figure 3. Fault 1. (a) Photograph of Fault 1 surface showing undulations consistent with strike-slip kinematics. (b) Riedel-shear fractures (indicated with green arrows) and fault slickenlines along Fault 1. (c) Detail of slickenlines (indicated with blue arrows) on the polished Fault 1 surface indicating strike-slip motion. (d) High-resolution scan image of polished hand sample F1A (across Fault 1), showing zonation with undulated boundary. (e) High-resolution scan image of polished hand sample F1B (across Fault 1), highlighting an ultrathin (<1 mm) ultracataclastic band above the undeformed host rock. (f) Optical microphotograph (plane-polarized light) showing the slip surface (SS) truncating a calcite vein and carbonate clasts; in this area, the SS transitions into a slip zone (SZ) is characterized by an ultracataclastic band. (g) Higher-magnification optical microphotograph (cross-polarized light) highlighting the ultracataclastic band and blackish, anastomosed sub-bands within the SZ (Fault 1). Lower-hemisphere Schmidt nets in (a) and (b) show fault surface orientation with slickenline direction.

21699356, 2026, 5, Downloaded from https://agupubs.onlinelibrary.wiley.com/doi/10.1029/2026JB033855 by Andrea Billi - University Di Roma La Sapienza , Wiley Online Library on [14/05/2026]. See the Terms and Conditions (https://onlinelibrary.wiley.com/terms-and-conditions) on Wiley Online Library for rules of use; OA articles are governed by the applicable Creative Commons License

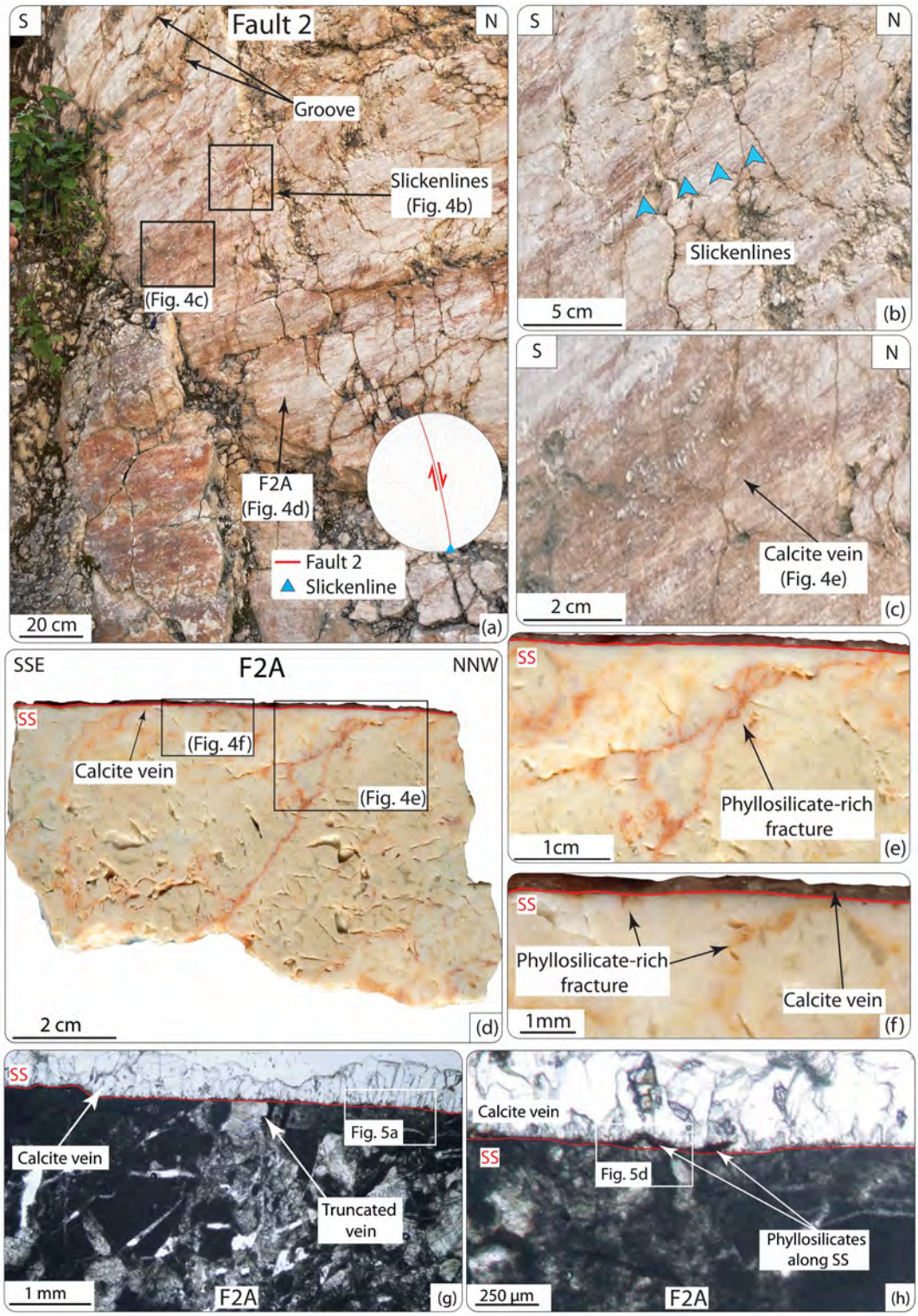

Figure 4. Fault 2. (a) Photograph of Fault 2 surface. Sample location (sample F2) is also shown. (b) Detail of slickenlines (indicated with blue arrows) on Fault 2 surface, indicating strike-slip motion. (c) Detail of the calcite vein with reddish coating decorating Fault 2 surface. (d) High-resolution scan image of polished hand sample F2. (e) Detail of the reddish phyllosilicate-rich fracture below the slip surface (SS). Note that the phyllosilicate-rich fracture departs from the SS forming an angle of 30–45°. The reddish phyllosilicate-rich fracture forms indeed a local network of fracture with different orientations. (f) Detail of the calcite vein with reddish coating, decorating the SS and accompanied by phyllosilicate-rich fracture below the SS. (g) Optical microphotograph (plane-polarized light) showing a truncated calcite vein along the Fault 2 surface. See also the calcite vein decorating the fault surface on one side (above). (h) Detail (plane-polarized light) of the calcite vein decorating the SS (Fault 2). Schmidt nets (lower hemisphere projection) in panel (a) illustrate fault orientation and slickenline direction.

21699356, 2026, 5, Downloaded from https://agupubs.onlinelibrary.wiley.com/doi/10.1029/2026JB033855 by Andrea Billi - University Di Roma La Sapienza , Wiley Online Library on [14/05/2026]. See the Terms and Conditions (https://onlinelibrary.wiley.com/terms-and-conditions) on Wiley Online Library for rules of use; OA articles are governed by the applicable Creative Commons License

21699356, 2026, 5, Downloaded from https://agupubs.onlinelibrary.wiley.com/doi/10.1029/2026JB033855 by Andrea Billi - University Di Roma La Sapienza , Wiley Online Library on [14/05/2026]. See the Terms and Conditions (https://onlinelibrary.wiley.com/terms-and-conditions) on Wiley Online Library for rules of use; OA articles are governed by the applicable Creative Commons License

The best-preserved fault surface (Fault 1; Figure 3) belongs to the ENE–WSW set and dips 65° to the SSE. It displays slickenlines, grooves, calcite slickenfibers, and Riedel shear planes (Figures 3a–3c), indicating left-lateral strike-slip motion. Grooves trend ENE-WSW (N76°), with a plunge of 16° toward the *E*, and define fault surface undulations (Figure 3a). Riedel shear planes strike NE–SW and dip 80°–84° toward SE (Figure 3b). Two samples (F1A, F1B) were collected from these fault surfaces and analyzed using SEM/FESEM, EPMA, and XRD (Figures 3d and 3e).

Sample F1A is a fault breccia with four distinct bands (Bands a–d in Figure 3d), whose cumulative thickness is 8 cm. These bands exhibit undulating contacts, color variation, and contrasts in fracture intensity. They contain rounded clasts from millimeters to ∼1 cm (Figure 3d). The investigated faults are hosted within the Monte Spigno Fm., which is predominantly composed of rounded to lobate oolitic–oncolitic carbonate grainstones, with grain sizes ranging from submillimetric to centimetric. Sample F1B shows a sharp contact between an ultrafine-grained ultracataclastic band (<1 mm) and the host rock. Beneath the ultracataclastic band, the sample is poorly deformed, and the original texture of the platform carbonate is preserved (Figure 3e).

A second well-exposed fault (Fault 2; Figure 4) belongs to the N–S-striking set and is located along the quarry's southeastern wall (Figures 2a and 4a). It dips 85° toward ENE and displays slickenlines, grooves, and calcite slickenfibers (Figures 4a and 4b), indicating right-lateral strike-slip motion. A ∼0.5 cm thick calcite vein decorates parts of the SS, preserving slickenlines indicative of strike-slip motion (Figures 4b and 4c). Two samples (F2A and F2B) were collected from this SS for optical, SEM/FESEM, EPMA, and XRD analyses (Figures 2b, 4a, and 4d). On the western side of the fault, in the first few millimeters from the SS, micrometric phyllosilicate-rich fractures are present (Figures 4e and 4f). These fractures mostly emanate from the SS, lying at low angle with respect to the SS itself (Figure 4d). Just above the SS (eastern side), the calcite vein shows a distinct reddish color (Figure 4f).

4.1.2. Optical Microscope Analyses

Optical microscopy of fault rock samples (F1A, F1B, and F2A) shows fault breccias below the SSs (Figures 3f, 3g, 4g, and 4h). These breccias are composed of millimeter-sized angular to subangular clasts embedded in a fine-grained microcrystalline calcite matrix (Figure 3g) and are crosscut by randomly oriented fractures and calcite veins (Figures 3f and 4g). The fault surfaces appear as sharp surfaces that truncate both clasts and vein fragments (Figures 3f and 4g), with locally preserved ultracataclastic patches (Figures 3f and 3g).

Sample F1B shows an ultracataclastic band composed of dark, very fine-grained material. The contact between the ultracataclastic band and the host rock is subparallel to the SS. This contact is sharp but undulated at the microscale (Figures 3f and 3g). The ultracataclastic band reaches a maximum thickness of ∼200 μm and contains anastomosed and undulating blackish ultracataclastic sub-bands (Figures 3f and 3g). Laterally, the SS broadens into a more diffuse SZ, which includes the above mentioned ultracataclastic band and where the discrete SS is no longer clearly defined (Figures 3e–3g).

In sample F2A (Fault 2), a calcite vein up to ∼0.5 mm thick is observed along the eastern side of the SS (Figures 4g and 4h). Localized phyllosilicate microlayers also occur along the SS in this sample (Figure 4h).

4.1.3. FESEM-EDS and EPMA Analyses

FESEM analysis revealed that the SSs exhibit an undulating geometry parallel to the slip direction—at the FESEM observation scale—with evidence of truncated clasts (Figures 5a–5e). Phyllosilicate microlayers consistently occur along the SSs (Figures 5b–5f). The local undulated nature of the SS is consistent with natural and experimental SS morphologies in carbonate faults documented by FESEM (see Figures 4a and 4d in Siman-Tov et al., 2013, Figure 5a in Violay et al., 2013, Figures 7d and 9e in Bullock et al., 2015; and Figures 2a and 3 in Curzi et al., 2026). The phyllosilicate layers, up to ∼15 μm thick, are typically parallel to the SSs (Figures 5b, 5d, 5e, and 6a) and occasionally appear as isolated pockets (Figure 5c; Figure S1a in Supporting Information S1).

Phyllosilicates also occur in fractures ranging from 5 to 30 μm in thickness that depart from the SSs into the adjacent host rock (Figures 5d and 6a–6c, and Figures S2–S8 in Supporting Information S1). Locally, these fractures form mesh-like network (producing breccias or incipient breccias), that branch outward from the SS, showing little to no systematic orientation in an absolute reference frame or relative to the SSs (Figures S4–S6 and S8 in Supporting Information S1). These fractures can propagate into well-developed brecciated microdomains

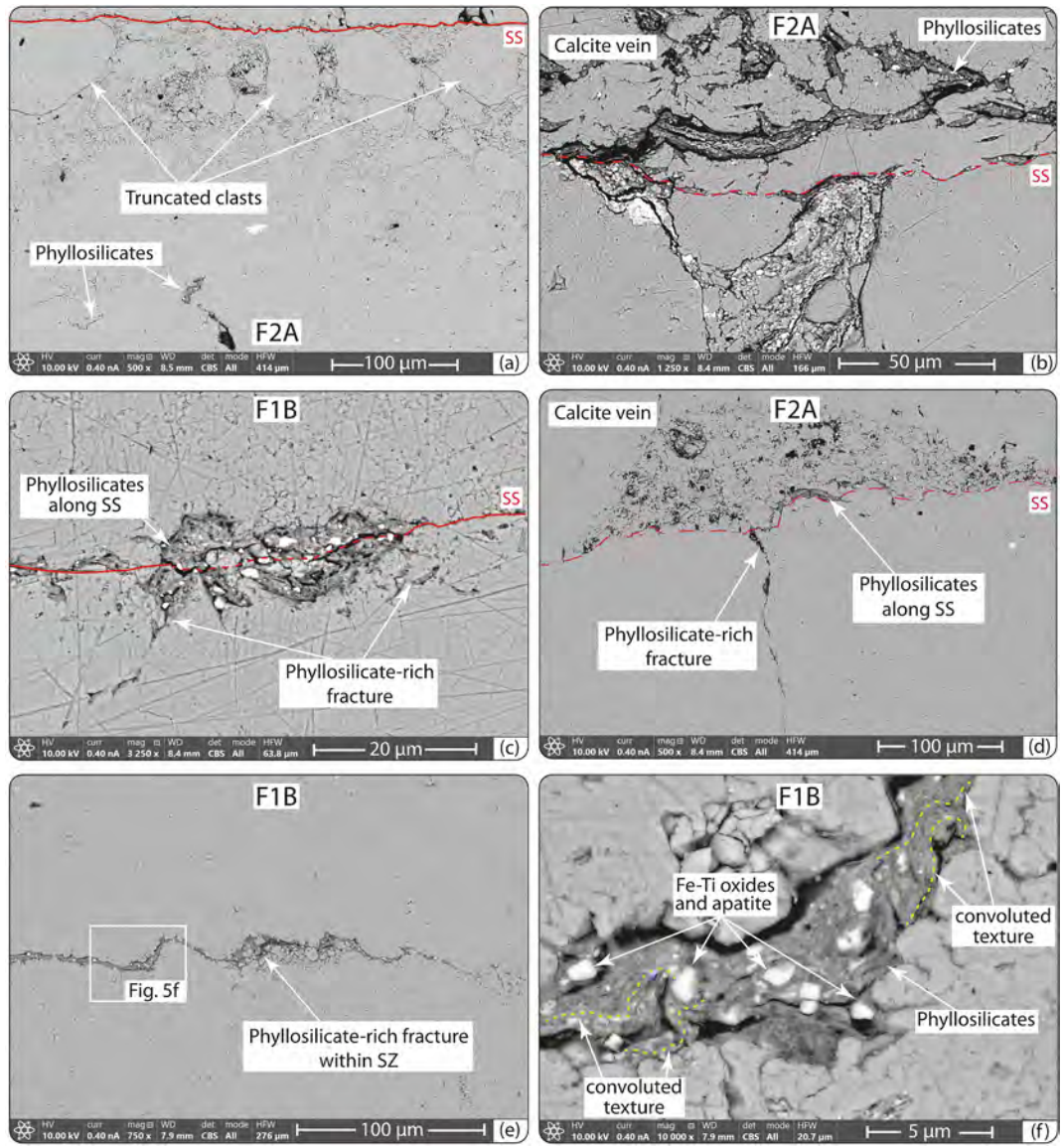

Figure 5. Scanning Electron Microscopy images of the slip surface (SS). (a) SS in sample F2A showing truncated host-rock clasts and phyllosilicates (Fault 2). (b) Detail of the SS in sample F2A highlighting phyllosilicates occurring along the SS and in the adjacent material above and below it (Fault 2). (c) Phyllosilicates along the SS in sample F1B (Fault 1), associated with a phyllosilicate-rich fracture. (d) Detail of the SS in sample F2A showing phyllosilicates both along the SS and within a phyllosilicate-rich fracture departing from the SS into the host rock (Fault 2). (e) Phyllosilicate-rich fracture within the slip zone (SZ) in sample F1B (Fault 1). (f) High-magnification view of phyllosilicates within the SZ in sample F1B (Fault 1), showing convoluted textures and associated Fe–Ti oxides and apatite. See image location in Figures 3g and 4h.

containing isolated clasts embedded in a phyllosilicate matrix with no substantial evidence of dissolution (e.g., no embayed clasts; Figures 6d, Figures S1e, S4–S8 in Supporting Information S1). The clasts of these breccias can be from angular or subangular to lobed or rounded, the latter (Figure 6d) probably coinciding with the original oolites-oncolites of the host rock or associated with abrasion due to mechanical transport.

Some fractures also widen toward the SS and progressively taper into the surrounding host rock (Figure S2 in Supporting Information S1). Phyllosilicates are not continuously distributed along the fractures; instead, they occur discontinuously and are often localized in the segments closest to the SSs (Figures S1f, S3, S4, S7, S8 in Supporting Information S1).

21699356, 2026, 5, Downloaded from https://agupubs.onlinelibrary.wiley.com/doi/10.1029/2026JB033855 by Andrea Billi - University Di Roma La Sapienza , Wiley Online Library on [14/05/2026]. See the Terms and Conditions (https://onlinelibrary.wiley.com/terms-and-conditions) on Wiley Online Library for rules of use; OA articles are governed by the applicable Creative Commons License

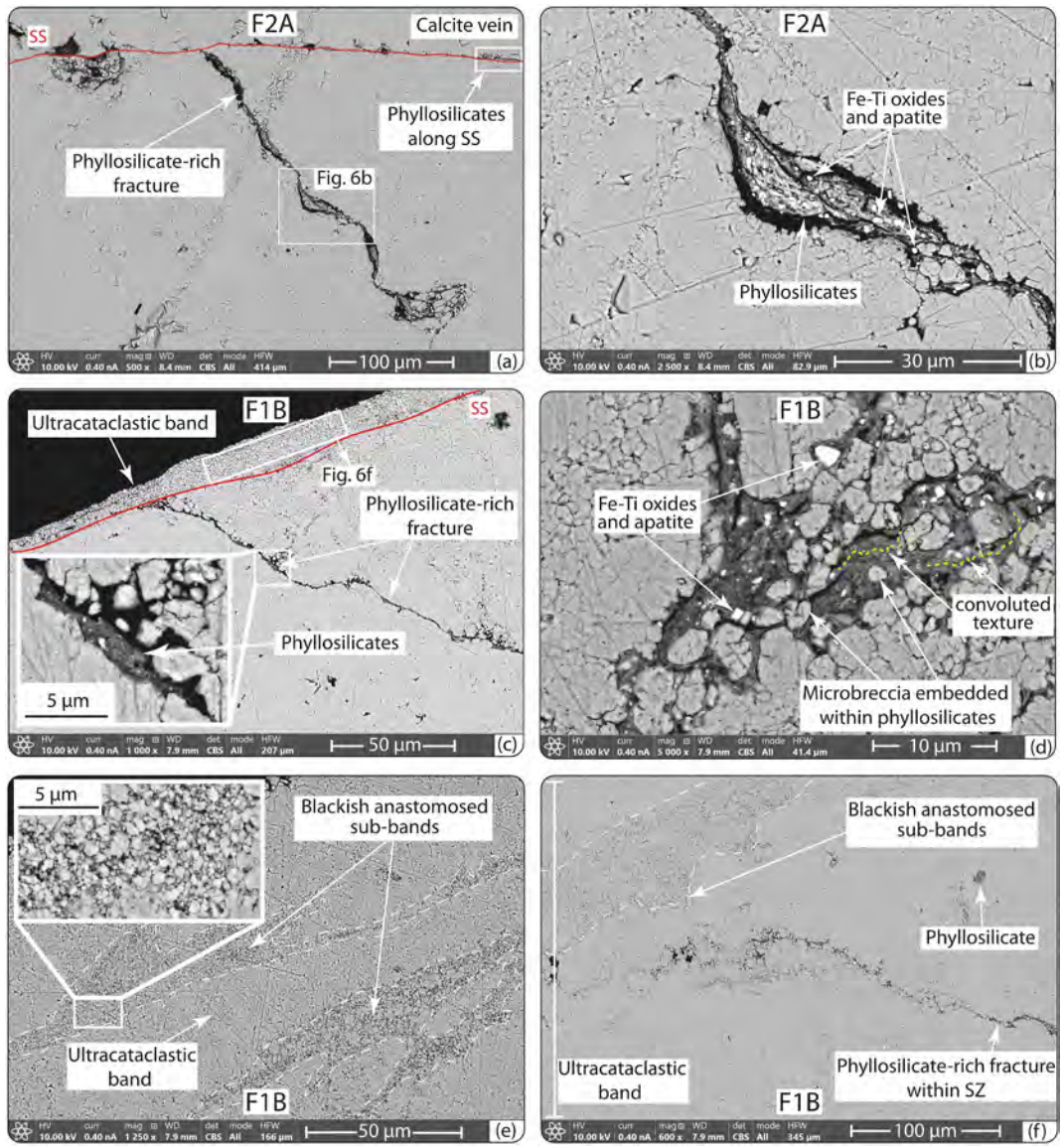

Figure 6. Scanning Electron Microscopy images of the sampled slip surfaces (SSs). (a) Phyllosilicates along the SS and phyllosilicate-rich fracture departing from the SS into the host rock (Fault 2). (b) High-magnification view of phyllosilicates within phyllosilicate-rich fracture (Fault 2). (c) Ultracataclastic band on one side of the SS in sample F1B, featuring a phyllosilicate-rich fracture (Fault 1). (d) Microbreccia composed of host rock limestone isolated clasts embedded within phyllosilicates along a phyllosilicate-rich fracture in sample F1B (Fault 1). (e) Ultracataclastic band and blackish anastomosed sub-bands occurring within the slip zone (Fault 1). (f) Ultracataclastic band containing a blackish anastomosed sub-band within the SZ; phyllosilicates may occur as isolated patches and as phyllosilicate-rich fractures. (Fault 1). See image location in Figure 3g.

Both phyllosilicate layers along the SSs and those within fractures departing from the SSs contain angular to sub-rounded micrometric carbonate clasts, euhedral Fe- and Ti-oxides, apatite, and fluorapatite, all embedded in a phyllosilicate-rich matrix that locally exhibits a convoluted texture, usually enveloping the clasts themselves (Figures 5f, 6b, and 6d). The clasts, in turn, are rarely in contact (Figures 5c, 5e, 5f, 6b–6d, Figures S4 and S8 in Supporting Information S1). Complete micro-scale (FESEM) mapping of phyllosilicate-rich fractures is in Figures S2–S8 in Supporting Information S1.

In places, fracture margins display a tight, sutured morphology (Figures S3–S8 in Supporting Information S1) reminiscent of pressure-solution seams. However, we do not observe further diagnostic evidence of pressure

21699356, 2026, 5, Downloaded from https://agupubs.onlinelibrary.wiley.com/doi/10.1029/2026JB033855 by Andrea Billi - University Di Roma La Sapienza , Wiley Online Library on [14/05/2026]. See the Terms and Conditions (https://onlinelibrary.wiley.com/terms-and-conditions) on Wiley Online Library for rules of use; OA articles are governed by the applicable Creative Commons License

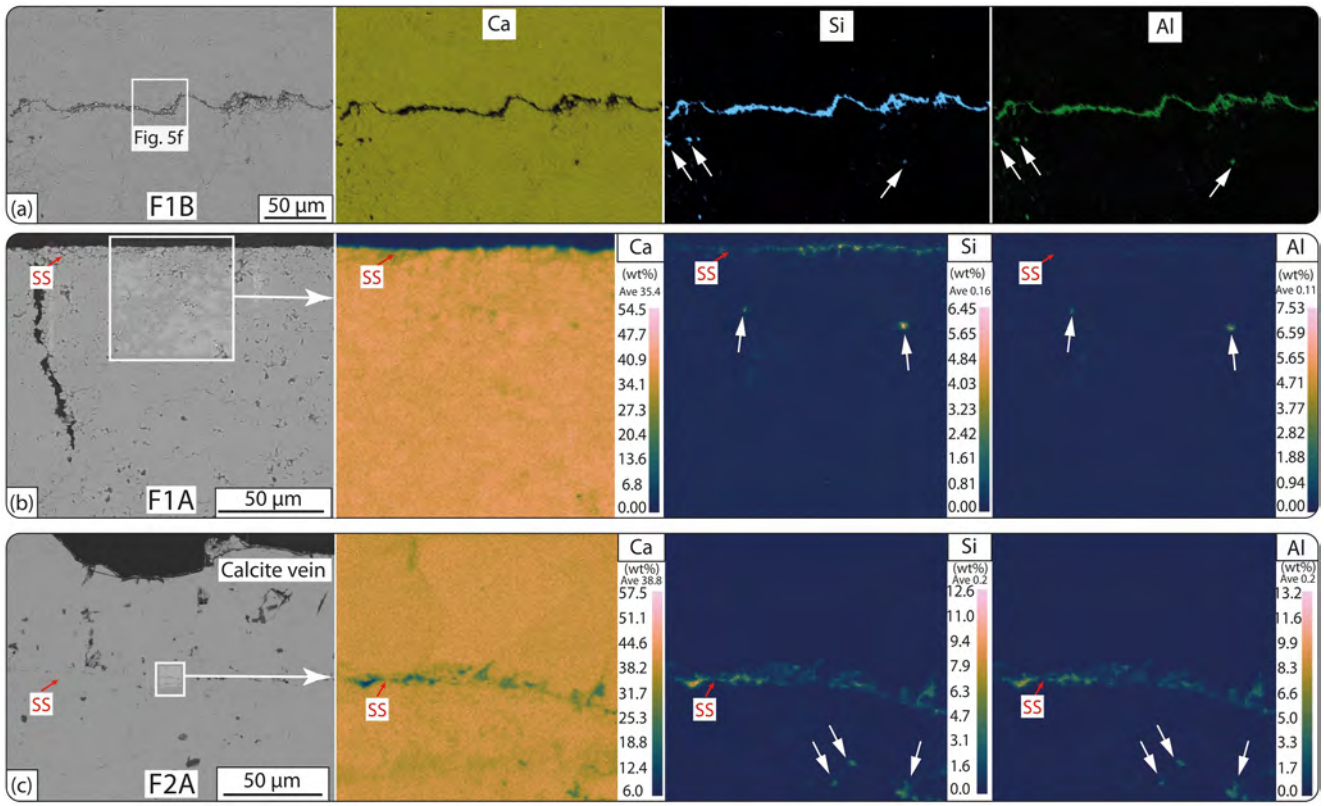

Figure 7. (a) Energy-dispersive spectroscopy element maps of the slip zone (SZ) in sample F1B showing decreased Ca (wt%) and increased Si and Al along a phyllosilicate layer within the SZ (Fault 1). (b) EPMA chemical maps of the slip surface (SS) in sample F1A, highlighting a decrease in Ca (wt%) and an increase in Si and Al contents (Fault 1). (c) EPMA chemical maps of the SS in sample F2A, showing a decrease in Ca (wt%) accompanied by Si and Al increase (Fault 2). Note the localized spots of elevated Si and Al contents located away from the SS (white arrows).

solution (e.g., embayed grains and stylolitic interpenetrations) along these margins (Figures 6d, Figures S1e, S4–S8 in Supporting Information S1).

Phyllosilicates in the host rock a few centimeters away from the SS are rare to absent (Figure S9 in Supporting Information S1). Where present, they occur only within intergranular pores proximal to the SS and show no microstructural evidence of deformation (Figures S10a, S10d in Supporting Information S1). Also in this fault host rock, carbonate clasts show no evidence of significant dissolution (i.e., embayed clasts; Figure S10a, S10d in Supporting Information S1). Additionally, Fe–Ti oxides and apatite are nearly absent in the host rock (Figures S10b, S10c, S10e, S10f in Supporting Information S1).

The ultracataclastic band observed in sample F1B (Figures 3e and Figure S11 in Supporting Information S1), which appears as dark sub-bands under the optical microscope (Figures 3f and 3g), is composed of fine-grained carbonates (<5 µm; Figures 6c and 6e). FESEM analysis shows that these dark sub-bands are 20–50 µm thick and consist of anastomosed bands of carbonate clasts up to ~2 µm in diameter (Figures 6e and 6f and Figure S11 in Supporting Information S1).

EDS and EPMA analyses show systematic enrichment in Si and Al along the SS and along the contact between the host rock and the ultracataclastic domain, coupled with a reduction in Ca, consistent with phyllosilicate concentration (Figure 7). Localized high-Si/Al zones are occasionally observed 30–50 µm far from the SS (Figure 7). F1B and F2A samples exhibit Fe and K enrichment in correspondence of the highest concentration of Si and Al (Figure S12 in Supporting Information S1). Additional elemental maps and interpretations are provided in the (Figures S12 and S13 in Supporting Information S1).

21699356, 2026, 5, Downloaded from https://agupubs.onlinelibrary.wiley.com/doi/10.1029/2026JB033855 by Andrea Billi - University Di Roma La Sapienza , Wiley Online Library on [14/05/2026]. See the Terms and Conditions (https://onlinelibrary.wiley.com/terms-and-conditions) on Wiley Online Library for rules of use; OA articles are governed by the applicable Creative Commons License

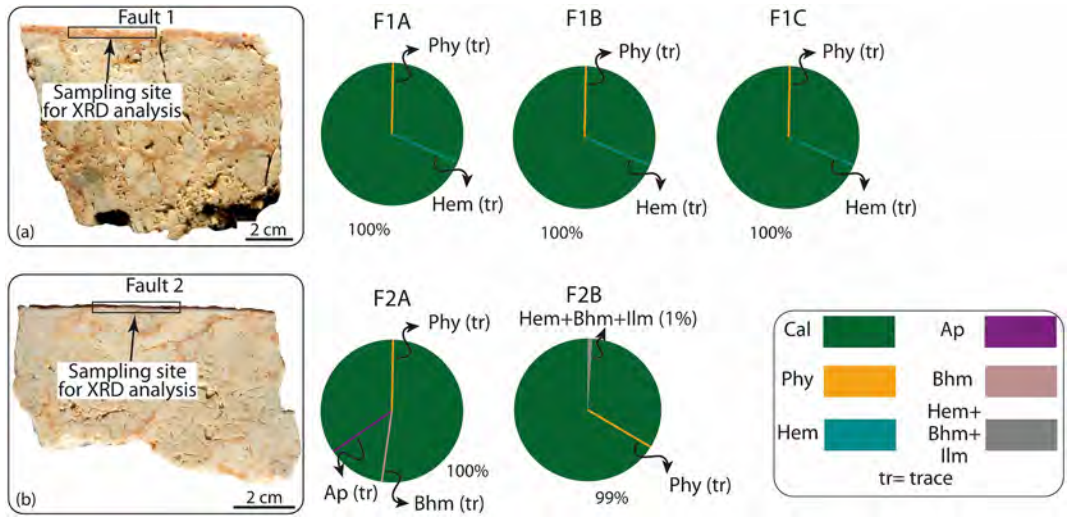

Figure 8. Photographs of hand samples from Fault 1 and Fault 2 (left) and associated mineralogical assemblage obtained from X-ray diffraction analyses on these samples (right). (a) Fault 1; (b) Fault 2. Pie charts show the mineral content. Note that other minerals besides calcite, in particular phyllosilicates, are only in trace amounts. See Figure 1 for sampling locations. Cal = calcite; Phy = phyllosilicates; Hem = hematite; Ap = Fluorapatite; Bhm = boehmite; Ilm = ilmenite.

4.1.4. XRD Analysis

XRD results on SSs are presented in Figure 8 and summarized in Table S2 in Supporting Information S1. The three samples from the SS of Fault 1 (F1A, F1B, and F1C; Figure 8a) consist entirely of calcite (100 wt%) with trace amounts (i.e., ≤1 wt% detection limit) of clay minerals (illite) and Fe-oxides (hematite). The two samples from the SS of Fault 2 (F2A and F2B; Figure 8b) mainly contain calcite (99%–100%), along with boehmite, hematite, and ilmenite (up to 1%), as well as trace amounts of clay minerals (illite and kaolinite) and fluorapatite.

4.2. Analysis of Phyllosilicates and Their Provenance

The unexpected occurrence of phyllosilicates along the analyzed SSs and in fractures emanating from them (Figures 5 and 6) calls for further investigation to constrain their origin in an otherwise phyllosilicate-poor or -free carbonate platform deposits (Figure 8). To this aim, we first reviewed the literature on the stratigraphy of the Gargano Promontory in search of potential phyllosilicate-bearing sources. We then conducted additional field surveys to assess the presence of phyllosilicate-rich layers near the studied faults and to collect samples for XRD analysis. Results are reported below.

4.2.1. Literature Analysis

A review of the Gargano lithostratigraphy and regional geology (Cotecchia & Canitano, 1954; Crescenti & Vighi, 1964; Martinis & Pieri, 1964; Morsilli & Bosellini, 1997; Bosellini et al., 1999; Morsilli, 2016; Del Viscio et al., 2021; Borrelli et al., 2023; ViDEPI Project) highlights some possible external sources (since the Monte Spigno Fm. host rock is virtually devoid of phyllosilicates; Table S2 in Supporting Information S1) for the clay minerals observed along the MF SSs (see log in Figure 1c for stratigraphic localization):

1. San Giovanni Rotondo Fm. (Lower Cretaceous). The closest potential source is represented by centimeters-thick, clay-rich interbeds within the San Giovanni Rotondo Fm., deposited in an inner-platform carbonate setting (Cremonini et al., 1971; Bosellini et al., 1999; Morsilli, 2016; Del Viscio et al., 2021; Figure 1b).
2. Marne a Fucoidi Fm. (Lower Cretaceous). This marly-limestone unit, stratigraphically equivalent to the Monte Spigno Fm. (the host unit of the investigated fault rocks) represents another potential phyllosilicate-bearing source in the study area (Cremonini et al., 1971; Bosellini et al., 1999; Morsilli, 2016; Del Viscio et al., 2021; Figure 1b).
3. Anidriti di Burano Fm. (Triassic). Below the Monte Spigno Fm., the most likely stratigraphic source of phyllosilicates is the Triassic Anidriti di Burano Fm. Exploration wells (Foresta Umbra 1 and Gargano 1) document thin argillaceous/shaly layers interbedded with dolostones and anhydrites (Martinis & Pieri, 1964;

21699356, 2026, 5, Downloaded from https://agupubs.onlinelibrary.wiley.com/doi/10.1029/2026JB033855 by Andrea Billi - University Di Roma La Sapienza , Wiley Online Library on [14/05/2026]. See the Terms and Conditions (https://onlinelibrary.wiley.com/terms-and-conditions) on Wiley Online Library for rules of use; OA articles are governed by the applicable Creative Commons License

Borrelli et al., 2023; ViDEPI Project). Argillaceous material was described in dark, bituminous Triassic marly limestones at Punta delle Pietre Nere (Cotecchia & Canitano, 1954; Figure 1b), although coastal erosion and anthropogenic disturbance currently prevent sampling and detailed characterization. Similar argillaceous layers may occur at Triassic levels beneath the investigated area.

4. *Terra rossa* infills. At a broader scale, the Apulian Platform carbonates exposed in the Gargano Promontory are pervasively karstified and locally filled by *terra rossa* deposits enriched in Fe-oxides and oxyhydroxide (hematite, goethite) and phyllosilicates (kaolinite, illite; Vingiani et al., 2018; Figure 2b). These deposits are frequent also in and around the study area.

4.2.2. Field Survey and Sampling

Building on the literature review, we identified four potential sources of phyllosilicates within the study area and across the Gargano Promontory: *terra rossa* deposits, the San Giovanni Rotondo and Marne a Fucoidi fms., as well as the Monte Spigno Fm., which constitutes the host rock of the studied faults. We surveyed representative exposures and collected four *terra rossa* samples within the quarry (F1F, F1G, F1H, F1K; Figures 1b and 2b), two samples of undeformed Monte Spigno Fm. remote host rock ∼1 km northwest of the quarry (MS1, MS2; Figure 1b), two clay-rich samples from the San Giovanni Rotondo Fm. ∼15 km west of the study area (SGR1, SGR2; Figure 1b), and one sample from the Marne a Fucoidi Fm. ∼7 km east of the study area (FUC1; Figure 1b). Sampling locations are shown in Figures 1b and 9. As noted above, the Triassic clay-rich rocks cannot be sampled, as they have been encountered only in deep exploratory wells or at the Punta delle Pietre Nere outcrop, which is now inaccessible or no longer extant.

4.2.3. XRD Analysis

XRD analysis on the above-mentioned additional samples shows that the Monte Spigno remote host rock (MS1 and MS2) is composed entirely of calcite (100 wt%) with trace amounts (i.e., <1 wt%) of quartz, boehmite, and anatase (Figure 9a and Table S2 in Supporting Information S1). The four samples from the *terra rossa* deposits (F1F, F1G, F1H, F1K) are primarily composed of calcite (70%–99%), with subordinate contents of boehmite (up to 11%), gibbsite (from 3% to 6%), kaolinite (1%–9%) and hematite (from traces to 2%) and minor amounts of illite (1%–2%) and anatase (<2%). Accessory minerals include fluorapatite (up to 1%) as well as quartz and rutile in trace amounts (Figure 9b and Table S2 in Supporting Information S1). The clay-rich beds from the San Giovanni Rotondo Fm. are composed of calcite (68%–82%), phyllosilicates (kaolinite, illite/muscovite, 18%–32%), and trace amounts of quartz, anatase, and dolomite (Figure 9c and Table S2 in Supporting Information S1). The clay-rich bed from the Marne a Fucoidi Fm. exhibits calcite (41%), phyllosilicates (smectite, mixed layered minerals, illite/muscovite, 46%), quartz (12%), K-feldspar (1%), and trace amounts of hematite and anatase (Figure 9d and Table S2 in Supporting Information S1).

5. Discussion

5.1. Unexpected Presence of Phyllosilicates Along the MF

The central finding of this study is the unexpected occurrence of phyllosilicates along carbonate-hosted faults in a foreland setting dominated by platform carbonates, where clay minerals are otherwise absent or extremely limited. Comparable phyllosilicates along carbonate-hosted faults have been reported from post-orogenic extensional fault zones within the central Apennines fold-and-thrust belt (e.g., Bullock et al., 2014; Coppola et al., 2021; Smeraglia et al., 2016). In those orogenic contexts, however, the presence of phyllosilicates along faults is less surprising because phyllosilicate-rich siliciclastic units are widespread at different stratigraphic levels, particularly in the upper portions of the succession, where syn-orogenic turbiditic deposits are common. By contrast, the identification of such layers along the MF, in the Apulian carbonate foreland, is unprecedented. Notably, along the MF, phyllosilicates are not confined to SSs but also occur within arrays of fractures that systematically emanate from the SSs (Figures 5–6 and 10; Figures S2–S8 in Supporting Information S1).

5.2. Source of Phyllosilicates

At least three hypotheses can be considered regarding the origin of the phyllosilicates found along SSs and within the injection veins:

21699356, 2026, 5, Downloaded from https://agupubs.onlinelibrary.wiley.com/doi/10.1029/2026JB033855 by Andrea Billi - University Di Roma La Sapienza , Wiley Online Library on [14/05/2026]. See the Terms and Conditions (https://onlinelibrary.wiley.com/terms-and-conditions) on Wiley Online Library for rules of use; OA articles are governed by the applicable Creative Commons License

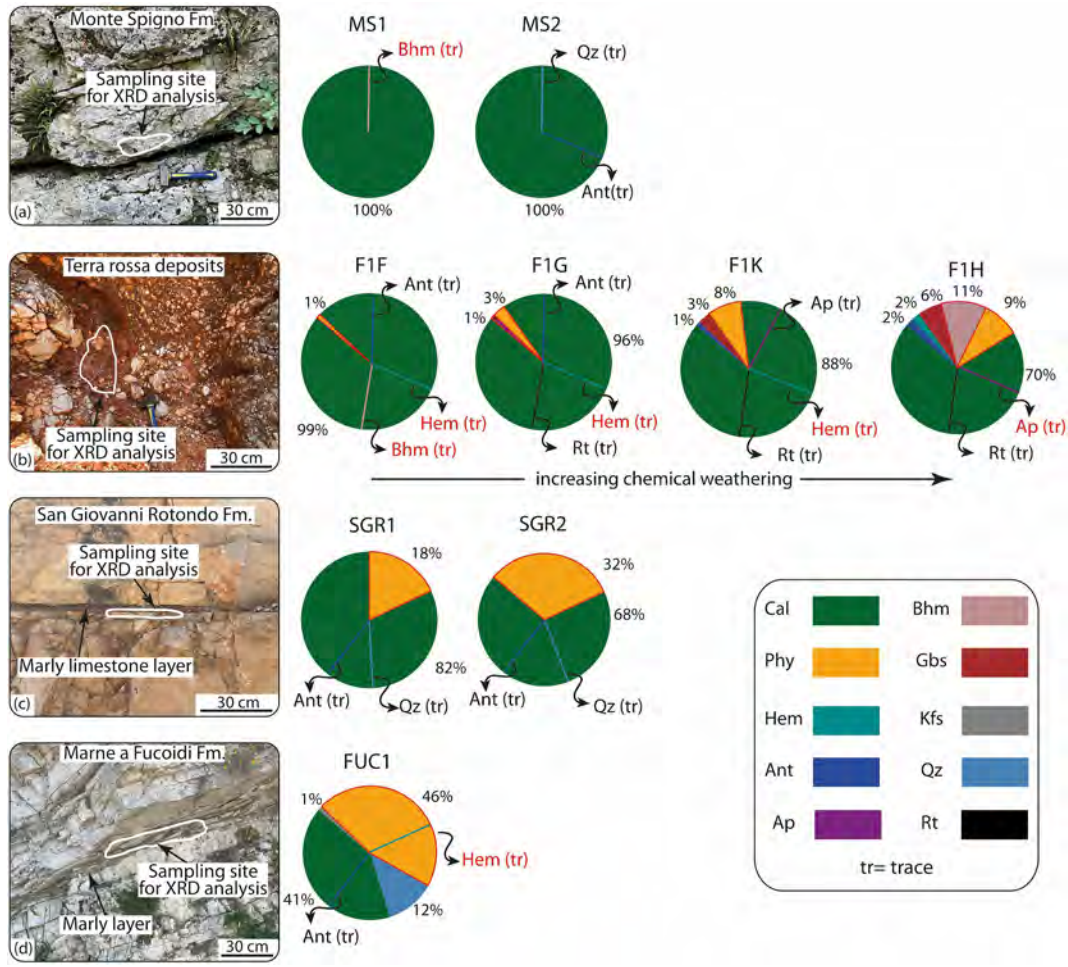

Figure 9. Field photographs of the sampled formations (left) and associated mineralogical assemblage obtained from X-ray diffraction analyses (right). (a) Monte Spigno Fm.; (b) *Terra Rossa* deposits; (c) San Giovanni Rotondo Fm.; (d) Marne a Fucoidi Fm. Pie charts show the mineral content. Minerals shown in red font and pie-chart slices with red outlines correspond to phases identified along fault zones. See Figure 1 for the sampling locations. Cal = calcite; Phy = phyllosilicates; Hem = hematite; Ant = anatase; Ap = Fluorapatite; Bhm = boehmite; Gbs = gibbsite; Kfs = k-feldspar; Qz = quartz; Rt = rutile.

1. The first attributes their occurrence to pressure-solution enrichment along stylolites within the host carbonate. However, the Monte Spigno Fm. host rock is demonstrably very poor in phyllosilicates (Figure 9a; Table S2 in Supporting Information S1), and stylolites containing clay minerals are extremely rare or absent, making this an unlikely source. Moreover, as discussed below (Section 5.3), several lines of microstructural, petrographic, and geometric evidence indicate that pressure-solution is not the dominant process responsible for the features observed along the MF.
2. The second and more plausible source is envisaged in the clay-rich beds within the San Giovanni Rotondo Fm. XRD analyses confirm the presence of illite and kaolinite in these stratigraphic levels, consistent with the phyllosilicates identified along the fault surfaces (Figures 9c and 9d; Table S2 in Supporting Information S1).
3. A third source is from the *terra rossa* deposits occurring along the MF (Figure 2b), whose mineralogical composition—illite, kaolinite, boehmite, hematite, and fluorapatite, among other phases (Figure 9b; Table S2 in Supporting Information S1)—partly matches that of the phyllosilicate microlayers along the studied faults (Figure 8; Table S2 in Supporting Information S1). In addition, XRD (and SEM–EDS) analyses indicate that the mineral assemblage of the phyllosilicate-rich material is similar to that of the *terra rossa* deposits exposed in the quarry, which occur in close spatial association with the fault zone. We therefore infer that *terra rossa* represents a primary local source for the phyllosilicates, later incorporated into the fault core and injected along SSs and related fractures.

21699356, 2026, 5, Downloaded from https://agupubs.onlinelibrary.wiley.com/doi/10.1029/2026JB033855 by Andrea Billi - University Di Roma La Sapienza , Wiley Online Library on [14/05/2026]. See the Terms and Conditions (https://onlinelibrary.wiley.com/terms-and-conditions) on Wiley Online Library for rules of use; OA articles are governed by the applicable Creative Commons License

21699356, 2026, 5, Downloaded from https://agupubs.onlinelibrary.wiley.com/doi/10.1029/2026JB033855 by Andrea Billi - University Di Roma La Sapienza , Wiley Online Library on [14/05/2026]. See the Terms and Conditions (https://onlinelibrary.wiley.com/terms-and-conditions) on Wiley Online Library for rules of use; OA articles are governed by the applicable Creative Commons License

Other sources for the phyllosilicates observed along SSs of the MF might be sought in deeper formations given the presence of argillaceous layers in Triassic rocks (e.g., Anidriti di Burano Fm.), encountered by exploration wells across the Gargano Promontory (Figure 1b). However, if sourced from Triassic units, transport distances to the faults within the Monte Spigno Fm. would have been substantially greater (on the order of several kilometers) than in the previously considered scenarios (*terra rossa* or the San Giovanni Rotondo Fm.). We therefore consider a Triassic origin for the phyllosilicates identified along the MF unlikely. Moreover, we consider the Marne a Fucoidi Fm. an unlikely source of the phyllosilicates identified along the SS, because its mineral assemblage differs from that observed along the SS (Table S2 in Supporting Information S1).

5.3. Fluid-Assisted Transport and Accumulation of Phyllosilicates

Several transport pathways from source rocks to fault surfaces can be envisaged, involving both mechanical and chemical processes. These may include (a) physical entrainment, infiltration, and/or smearing of clay-rich material along SSs enhanced by fluid circulation (Chen et al., 2013; Smeraglia et al., 2016), and (b) authigenic precipitation from circulating fluids (Schleicher & Jurado, 2019; Figures 5f, 6b, and 6d). Among these alternatives, our observations are most consistent with the former, mechanically driven process. In particular, the co-occurrence of minerals such as kaolinite and illite is difficult to reconcile with co-precipitation from a single fluid under uniform physico-chemical conditions, thereby arguing against a dominant authigenic origin. The rounded morphology of the microbreccia clasts (Figure 6d) may further suggest abrasion during transport. In addition, the discontinuous distribution of phyllosilicates along the fractures supports localized transport and deposition rather than in situ precipitation.

The phyllosilicate-bearing infills display convolute fabrics and locally form a matrix that supports floating carbonate clasts as well as accessory phases (e.g., apatite and oxide grains). These textures are best explained by episodic injection of pressurized fluids. The overall geometry and internal organization of these structures are indeed consistent with injection veins described in other fault zones (Coppola et al., 2021; Gu et al., 2021). Several other observations support an injection interpretation: (a) phyllosilicates within the fractures display a predominantly convoluted fabric; (b) clasts in brecciated, phyllosilicate-rich fracture zones are typically matrix-supported by phyllosilicates and only rarely in mutual contact (Figures 5c, 5e, 5f, 6b–6d; Figure S4 and S8 in Supporting Information S1); (c) phyllosilicates occur discontinuously along the fractures (Figures S1f, S3, S4, S7, S8 in Supporting Information S1), consistent with localized mechanical deposition; (d) in several cases, phyllosilicate abundance is higher adjacent to the SSs and decreases away from them (Figures S3, S4, S7, S8 in Supporting Information S1); (e) phyllosilicate-rich fractures show variable orientations (both in absolute terms and relative to the SS) and commonly emanate from the SSs (Figures S4 and S8 in Supporting Information S1); (f) locally, these fractures transition into well-developed or incipient micro-brecciated domains branching off the SSs (Figure 6d, Figure S1e, S3–S8 in Supporting Information S1); and (g) in some cases, fracture aperture increases toward the SSs and progressively tapers into the host rock (Figure S2 in Supporting Information S1).

Taken together, these observations suggest that injection processes were the dominant mechanism driving phyllosilicate accumulation. By contrast, pressure solution, although theoretically feasible, unlikely played a primary role in phyllosilicate accumulation. Diagnostic pressure-solution microstructures are absent, and the observed fabrics are more readily explained by injection-related processes. Nevertheless, a minor pressure-solution component may have contributed locally, particularly to fracture nucleation. As noted above, the margins of some phyllosilicate-rich fractures are irregular and weakly serrated, consistent with incipient dissolution and compaction along some pre-existing discontinuities (Figure S3 in Supporting Information S1). We interpret these features as localized overprinting and/or inheritance from earlier pressure-solution seams rather than evidence that the phyllosilicate-rich layers represent primary pressure-solution residues. Accordingly, early pressure-solution seams and/or other pre-existing fractures may have acted as mechanical anisotropies and permeability pathways that were later reactivated during transient fluid overpressure, facilitating injection and accumulation of phyllosilicate-rich material. It is important to note, however, that although pressure-solution structures have previously been documented along the MF (Billi, 2003; Salvini et al., 1999), we did not observe a clear, systematic pattern of pressure-solution features in the immediate vicinity of the faults.

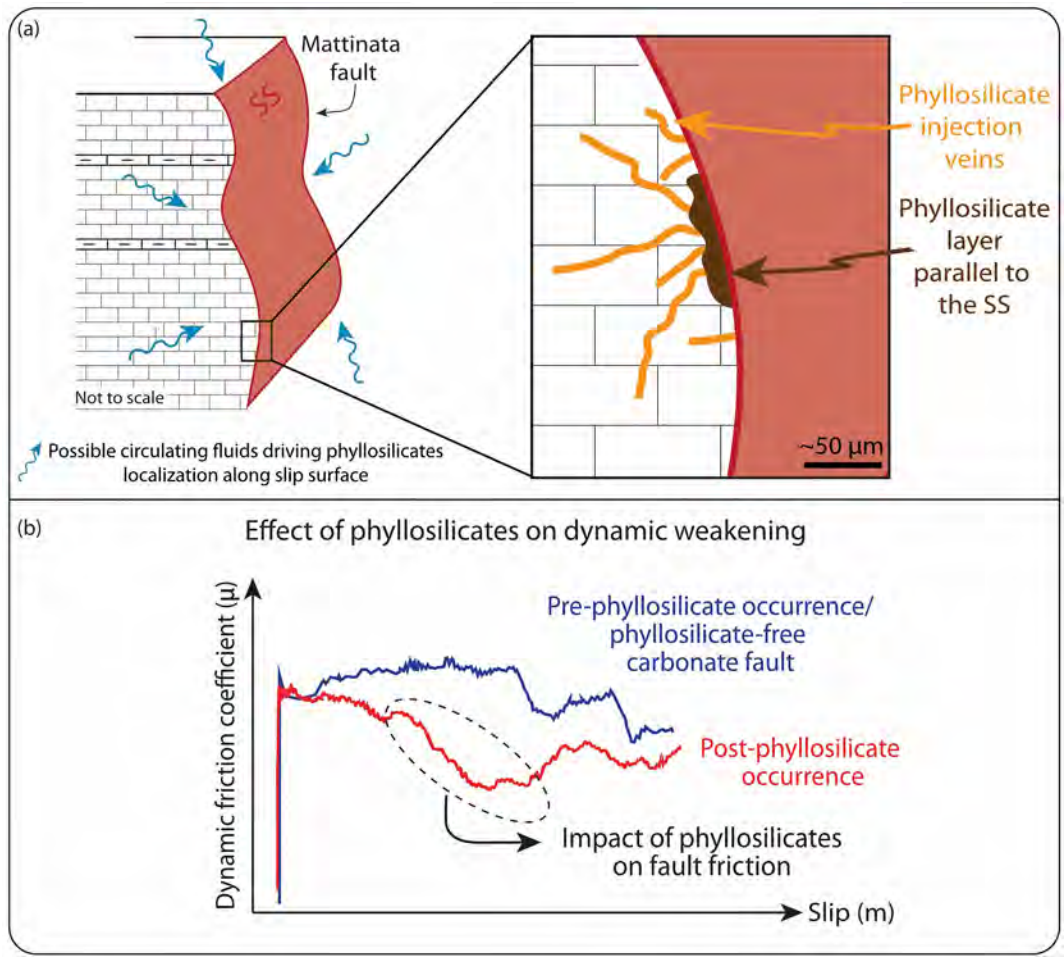

Figure 10. Schematic illustration of the Mattinata Fault and implications for fault mechanics. (a) Conceptual sketch (not to scale) of the fault surface, showing potential fluid-circulation pathways and their role in transporting phyllosilicates toward the fault. The enlarged box illustrates the microstructural configuration documented here, with phyllosilicate injection veins emanating from the fault surface and the development of a phyllosilicate-rich layer parallel to the slip surface (see Figures 5 and 6). (b) Effect of phyllosilicates on fault mechanics: laboratory-derived frictional behavior of carbonate faults (modified after Smeraglia, Billi, et al., 2017), comparing phyllosilicate-free (blue curve) and phyllosilicate-bearing (red curve) cases.

5.4. Evidence for Coseismic Fluid Pressurization

The occurrence of injection veins (Figures 4e, 5d, 6a, and 6c, Figures S2–S8 in Supporting Information S1) suggests that pressurized fluids accompanied the MF tectonic and/or seismic activity, facilitating the infiltration of phyllosilicates along SSs (Coppola et al., 2021; Gu et al., 2021; Rowe & Griffith, 2015; Uysal et al., 2011). Experimental constraints provide an independent line of support for this mechanism. High-velocity shear experiments on carbonates have produced injections of micrometer-scale carbonate grains dispersed within phyllosilicates under purely seismic conditions (Smeraglia, Billi, et al., 2017, Smeraglia, Bettucci, et al., 2017). On this basis, the occurrence of injection veins implies transient fluid pressurization along the SSs during coseismic slip, promoting injection into adjacent fractures (Coppola et al., 2021; Gu et al., 2021; Lin, 1996; Otsuki et al., 2005; Rowe & Griffith, 2015; Smeraglia, Bettucci, et al., 2017; Uysal et al., 2011). Thus, the main pulse of fluid pressurization likely occurred along the SSs or within the SZ themselves, most plausibly during seismic rupture events (Figure 10b).

5.5. Relevance for Seismic Faults and Laboratory Experiments

The unexpected occurrence of micrometric phyllosilicate layers along the MF has important implications for the mechanics of this active carbonate-hosted fault and for the interpretation of phyllosilicate-bearing high-velocity

21699356, 2026, 5, Downloaded from https://agupubs.onlinelibrary.wiley.com/doi/10.1029/2026JB033855 by Andrea Billi - University Di Roma La Sapienza , Wiley Online Library on [14/05/2026]. See the Terms and Conditions (https://onlinelibrary.wiley.com/terms-and-conditions) on Wiley Online Library for rules of use; OA articles are governed by the applicable Creative Commons License

friction experiments. Our observations show that externally sourced phyllosilicates can be selectively localized along SSs, even in a geological context almost devoid of clays. These unexpected phyllosilicate-rich layers imply that active and seismogenic faults can accumulate phyllosilicates even where the surrounding lithologies contain only trace amounts.

Experimental studies demonstrate that such localized enrichment is mechanically critical: when confined to narrow SSs, even ultra-low clay contents can produce large (i.e., from $\mu \approx 0.5$–0.8 to $\mu \approx 0.35$–0.40) reductions in dynamic friction and fault strength (Bullock et al., 2015; Smeraglia, Billi, et al., 2017) and lower fault-core stiffness at the nanoscale (Smeraglia, Bettucci, et al., 2017; Figure 10).

Moreover, high-velocity rotary-shear experiments also demonstrate that even minor amounts of phyllosilicate gouges along SSs can substantially enhance dynamic weakening. During seismic slip, phyllosilicates can facilitate thermal pressurization of pore fluids and drive extreme grain-size reduction down to the nanoscale (Boutareaud et al., 2012), both of which act to lower coseismic fault strength. We note that phyllosilicate along the studied SSs occur discontinuously and locally define an undulating geometry. Although this distribution may limit their influence on bulk or static fault strength, largely governed by asperities (e.g., Chen et al., 2020), our interpretation instead emphasizes dynamic weakening processes operating at seismic slip rates. Under such conditions, low-friction minerals can promote substantial friction reduction once slip is initiated. Such processes are documented in high-velocity experiments on kaolinite-bearing gouges (Brantut et al., 2008), which are partially comparable to those observed along the MF.

These experimental findings highlight a key implication for our natural case: fault weakening does not require a phyllosilicate-rich host rock, but rather the mechanical, chemical, and structural input of phyllosilicates along thin, localized SSs. This interpretation aligns with our observations at MF, where phyllosilicates are not inherited from the carbonate host rock but instead are localized through externally sourced injections and fluid-assisted transfer processes (Brantut et al., 2010).

A second key mechanical implication concerns the role of fluids. Our microstructural evidence—including ultracataclastic bands and clay-rich injection veins—indicates episodes of fluid pressure pulses during seismic slip. Convoluted textures occur both within the ultracataclasite and within injection veins/fractures, where phyllosilicates display fluidal fabrics and entrain floating carbonate clasts (Figures 5f, 6d–6f, Figure S11 in Supporting Information S1). Similar convoluted ultracataclastic bands and phyllosilicate within injections have been interpreted as the product of rapid pore fluid pressurization, as documented in natural faults and reproduced in high-velocity shear experiments (<1 m s^{-1}) (see Figure 6 in Smith et al., 2011, Figure 7 in Delle Piane et al., 2017, Figure 2d in Smeraglia, Billi, et al., 2017, and Figure 2e–2f in Smeraglia, Bettucci, et al., 2017). These pressurization events would have locally reduced effective normal stress, facilitated slip acceleration, and contributed to the development of ultracataclasite layers with very low frictional resistance.

Our results therefore emphasize a dual role for fluids: they can (a) transport and concentrate phyllosilicates along SSs, and (b) dynamically weaken the fault through transient pressurization.

Historical and instrumental records for the Gargano Promontory document moderate to large earthquakes ($Mw \leq 7$; Figure 1b), suggesting that efficient stress accumulation and release have occurred. In this context, the presence of phyllosilicates along SSs provides a viable mechanism for local and transient reduction of dynamic friction (Smeraglia, Billi, et al., 2017) and possibly for rupture propagation (Faulkner et al., 2011; Kirkpatrick et al., 2025). Moreover, the presence of injection veins implies that seismic slip was associated with fluid pressurization, raising the possibility that transient fluid pulses further influenced rupture propagation and even aftershock sequences (Smeraglia, Billi, et al., 2017, Smeraglia, Bettucci, et al., 2017).

Our multiscale structural observations are derived from a limited sector of the MF and are therefore intended to provide a process-based framework rather than a fault-wide characterization. Moreover, the direct transport of surficial materials such as *terra rossa* to seismogenic depths remains uncertain, and we do not imply that surface-derived material necessarily extends to depth along the MF. Instead, we suggest that analogous fluid-assisted transport and concentration of phyllosilicates may occur at depth, where alternative clay sources (e.g., deeper stratigraphic levels containing argillaceous material) are available, allowing similar weakening mechanisms to operate without requiring direct involvement of surface-derived material.

21699356, 2026, 5, Downloaded from https://agupubs.onlinelibrary.wiley.com/doi/10.1029/2026JB033855 by Andrea Billi - University Di Roma La Sapienza , Wiley Online Library on [14/05/2026]. See the Terms and Conditions (https://onlinelibrary.wiley.com/terms-and-conditions) on Wiley Online Library for rules of use; OA articles are governed by the applicable Creative Commons License

21699356, 2026, 5, Downloaded from https://agupubs.onlinelibrary.wiley.com/doi/10.1029/2026JB033855 by Andrea Billi - University Di Roma La Sapienza , Wiley Online Library on [14/05/2026]. See the Terms and Conditions (https://onlinelibrary.wiley.com/terms-and-conditions) on Wiley Online Library for rules of use; OA articles are governed by the applicable Creative Commons License

Beyond their implications for natural seismicity, the microstructures documented along the MF offer valuable constraints for designing the next generation of high-velocity friction experiments.

First, the presence of micrometric phyllosilicate layers and fluidal phyllosilicate–carbonate mixtures strongly suggests that future experiments on carbonate faults should explicitly incorporate externally sourced clays, rather than assuming carbonate–clay mineral mixtures as a closed system. Experiments that neglect externally introduced clay minerals may underestimate the fluid-assisted processes responsible for clay infiltration and accumulation, as documented in this study.

Second, the occurrence of phyllosilicate-filled injection veins indicates that fluid pressures during seismic slip may locally reach supra-hydrostatic values along the fault, sufficient to fracture the wall rock and injecting clay-bearing suspensions. However, most existing high-velocity experiments primarily reproduce fluid pressurization in closed or internally saturated systems and therefore do not fully capture the conditions inferred in our natural case. In particular, our observations suggest that transient external fluid pulses and open-system influx play a key role by injecting externally derived material (e.g., phyllosilicates) into the fault zone. Experimental investigations incorporating externally driven fluid pressurization and fluid injection processes are essential to reproduce the dynamics of natural fault conditions such as those documented along the MF.

Collectively, these findings highlight the importance of integrating mineralogical complexity, transient fluid processes, and multi-scale fault-rock textures into both modeling and laboratory approaches aimed at understanding the seismic cycle in carbonate foreland faults as well as in the upward propagation of seismic ruptures through carbonate rocks.

6. Conclusions

Our investigation of the MF shows that phyllosilicate microlayers can form along active faults even in an intrinsically clay-poor carbonate system. We document that micrometric layers of illite and kaolinite and associated injection veins localize along SSs indicating that even minor clay fraction can be localized during deformation. This process is best explained by open-system, fluid-assisted transport and transient pressurization during seismic slip, rather than by in situ derivation from the carbonate host rock.

This finding carries first-order mechanical implications. Concentration of phyllosilicates into microlayers theoretically can reduce the effective fault strength, promote slip localization, and—by lowering frictional resistance along the principal SS—facilitate rupture propagation toward the Earth's surface, potentially enhancing coseismic surface damage. In addition, the intimate association between clay-rich coatings and injection veins supports a scenario in which dynamic weakening is promoted by coseismic slip; for the MF, we specifically infer that clay-bearing injections represent a key field signature of transient, fluid-supported weakening during rapid slip.

Consequently, physical and numerical models of seismic faulting, particularly in carbonates, should not treat these systems as closed and clay-free by default. Instead, they should explicitly explore open-system endmembers in which phyllosilicates can be injected and smeared along SSs under both static (interseismic) and dynamic (coseismic) conditions, thus making localized weak microlayers coexist with a strong carbonate framework.

Recognizing and quantifying such cryptic, fluid-mediated clay focusing is therefore essential not only to refine fault-mechanics models in the Apulian foreland and elsewhere, but also to improve seismic hazard assessment in carbonate provinces worldwide, where apparently clean carbonate-hosted faults may nonetheless host mechanically critical, micrometer-scale weak interfaces.

Inclusion in Global Research Statement

This study was conducted entirely in Italy by authors affiliated with Italian institutions, and it did not involve international field campaigns or research partnerships with local or indigenous communities outside the authors' home context. Field observations and sampling in southern Italy were carried out in accordance with applicable regulations and site-access requirements. Accordingly, additional disclosures under the AGU "Inclusion in Global Research" policy are not applicable to this manuscript.

AI Tools Disclosure

During the preparation of this work the authors used ChatGPT to improve readability and fluency of the text. After using this tool/service, the authors reviewed and edited the content as needed. Hence, they take full responsibility for the content of the publication.

Conflict of Interest

The authors declare no conflicts of interest relevant to this study.

Availability Statement

The data set supporting this study is archived in Calvanelli et al. (2026). The repository includes the Supporting Information file, as well as high-resolution versions of the photomerged SEM mosaics presented in the Supporting Information (Figures S2–S8 in Supporting Information S1). It also contains the raw drone, FESEM-EDS, EPMA, and XRD data generated in this study. All files are provided under a Creative Commons Attribution 4.0 International (CC BY 4.0) license and are openly accessible without registration. Structural data were processed using Stereonet (Cardozo & Allmendinger, 2013), photogrammetric models were generated using Agisoft Metashape Professional (Agisoft LLC, 2026), and virtual outcrop interpretation was performed using Virtual Reality Geological Studio (Hodgetts et al., 2007).

Acknowledgments

This work was funded by Sapienza Progetti di Ateneo 2023 (E. Carminati, protocol RG123188913B2632), Progetto di Ateneo 2024 (M. Curzi, CUP: B83C25000880005), and was also carried out within the RETURN Extended Partnership, receiving funds from the European Union Next-GenerationEU (National Recovery and Resilience Plan—NRRP, Mission 4, Component 2, Investment 1.3—D.D. 1243 2/8/2022, PE0000005). We thank Domenico Mannetta for preparing thin sections, Tania Ruspandini for assistance with SEM analyses, Fabrizio Di Fiore, Manuela Nazzari, and Piergiorgio Scarlato for support with FESEM analyses. Lorenzo Monaco and Giovanni Gaglianone are thanked for assistance with EPMA and chemical analyses, respectively. We warmly thank the two anonymous reviewers for their constructive suggestions and the editors for their careful handling of the manuscript. Open access publishing facilitated by Consiglio Nazionale delle Ricerche, as part of the Wiley - CRUI-CARE agreement.

References

Agisoft LLC. (2026). Agisoft Metashape Professional (Version 1.8.5) [Software]. Retrieved from https://www.agisoft.com/

Argnani, A., Favalli, P., Frugoni, F., Gasperini, M., Ligi, M., Marani, M., et al. (1993). Foreland deformational pattern in the Southern Adriatic Sea. *Annals of Geophysics*, *36*(2), 24. https://doi.org/10.4401/ag-4279

Argnani, A., Rovere, M., & Bonazzi, C. (2009). Tectonics of the Mattinata fault, offshore south Gargano (southern Adriatic Sea, Italy): Implications for active deformation and seismotectonics in the foreland of the Southern Apennines. *Geological Society of America Bullettin*, *121*(9–10), 1421–1440. https://doi.org/10.1130/B26326.1

Bertotti, G., Casolari, E., & Picotti, V. (1999). The Gargano Promontory: A Neogene contractional belt within the Adriatic plate. *Terra Nova*, *11*(4), 168–173. https://doi.org/10.1046/j.1365-3121.1999.00243.x

Billi, A. (2003). Solution slip and separations on strike-slip fault zones: theory and application to the Mattinata Fault, Italy. *Journal of Structural Geology*, *25*(5), 703–715. https://doi.org/10.1016/s0191-8141(02)00077-9

Billi, A., Gambini, R., Nicolai, C., & Storti, F. (2007). Neogene-Quaternary intraforeland transpression along a Mesozoic platform-basin margin: The Gargano fault system, Adria, Italy. *Geosphere*, *3*(1), 1–15. https://doi.org/10.1130/GES00057.1

Billi, A., & Salvini, F. (2003). Development of systematic joints in response to flexure-related fibre stress in flexed foreland plates: The Apulian forebulge case history, Italy. *Journal of Geodynamics*, *36*(4), 523–536. https://doi.org/10.1016/S0264-3707(03)00086-3

Borrelli, M., Perri, E., Morsilli, M., & Critelli, S. (2023). Late Permian-Triassic sedimentary evolution of the Southern Adriatic area based on wells and cores analysis. *Marine and Petroleum Geology*, *150*, 106154. https://doi.org/10.1016/j.marpetgeo.2023.106154

Bosellini, A., Morsilli, M., & Neri, C. (1999). Long-term event stratigraphy of the Apulia Platform margin (Upper Jurassic to Eocene, Gargano, southern Italy). *Journal of Sedimentary Research*, *69*(6), 1241–1252. https://doi.org/10.2110/jsr.69.1241

Boutareaud, S., Hirose, T., Andréani, M., Pec, M., Calugaru, D. G., Boullier, A. M., & Doan, M. L. (2012). On the role of phyllosilicates on fault lubrication: Insight from micro-and nanostructural investigations on talc friction experiments. *Journal of Geophysical Research*, *117*(B8). https://doi.org/10.1029/2011JB009006

Brankman, C. M., & Aydin, A. (2004). Uplift and contractional deformation along a segmented strike-slip fault system: The Gargano Promontory, southern Italy. *Journal of Structural Geology*, *26*(5), 807–824. https://doi.org/10.1016/j.jsg.2003.08.018

Brantut, N., Schubnel, A., Corvisier, J., & Sarout, J. (2010). Thermochemical pressurization of faults during coseismic slip. *Journal of Geophysical Research*, *115*(B5). https://doi.org/10.1029/2009JB006533

Brantut, N., Schubnel, A., Rouzaud, J. N., Brunet, F., & Shimamoto, T. (2008). High-velocity frictional properties of a clay-bearing fault gouge and implications for earthquake mechanics. *Journal of Geophysical Research*, *113*(B10). https://doi.org/10.1029/2007JB005551

Bullock, R. J., De Paola, N., & Holdsworth, R. E. (2015). An experimental investigation into the role of phyllosilicate content on earthquake propagation during seismic slip in carbonate faults. *Journal of Geophysical Research: Solid Earth*, *120*(5), 3187–3207. https://doi.org/10.1002/2015JB011914

Bullock, R. J., De Paola, N., Holdsworth, R. E., & Trabucho-Alexandre, J. (2014). Lithological controls on the deformation mechanisms operating within carbonate-hosted faults during the seismic cycle. *Journal of Structural Geology*, *58*, 22–42. https://doi.org/10.1016/j.jsg.2013.10.008

Calvanelli, R., Aldega, L., Billi, A., Cavallo, A., Curzi, M., Mercuri, M., et al. (2026). Weakening processes in carbonate-hosted faults: Phyllosilicate microlayers and injections along the Mattinata fault (Southern Italy) [Dataset]. *Figshare*. https://doi.org/10.6084/m9.figshare.31996554

Camassi, R., Bernardini, F., Castelli, V., & Meletti, C. (2008). A 17th century destructive seismic crisis in the Gargano area: Its implications on the understanding of local seismicity. *Journal of Earthquake Engineering*, *12*(8), 1–23. https://doi.org/10.1080/13632460802212774

Cardozo, N., & Allmendinger, R. W. (2013). Spherical projections with OSXStereonet [Software]. *Computers and Geosciences*, *51*, 193–205. https://doi.org/10.1016/j.cageo.2012.07.021

Carminati, E., & Doglioni, C. (2005). Mediterranean tectonics. *Encyclopedia of Geology*, *2*, 135–146.

Carminati, E., Lustrino, M., & Doglioni, C. (2012). Geodynamic evolution of the central and western Mediterranean: Tectonics vs. igneous petrology constraints. *Tectonophysics*, *579*, 173–192. https://doi.org/10.1016/j.tecto.2012.01.026

Carpenter, B. M., Marone, C., & Saffer, D. M. (2011). Weakness of the San Andreas Fault revealed by samples from the active fault zone. *Nature Geoscience*, *4*(4), 251–254. https://doi.org/10.1038/NGEO1089

21699356, 2026, 5, Downloaded from https://agupubs.onlinelibrary.wiley.com/doi/10.1029/2026JB033855 by Andrea Billi - University Di Roma La Sapienza , Wiley Online Library on [14/05/2026]. See the Terms and Conditions (https://onlinelibrary.wiley.com/terms-and-conditions) on Wiley Online Library for rules of use; OA articles are governed by the applicable Creative Commons License

Chen, J., Yang, X., Ma, S., & Spiers, C. J. (2013). Mass removal and clay mineral dehydration/rehydration in carbonate-rich surface exposures of the 2008 Wenchuan Earthquake fault: Geochemical evidence and implications for fault zone evolution and coseismic slip. *Journal of Geophysical Research: Solid Earth*, *118*(2), 474–496. https://doi.org/10.1002/jgrb.50089

Chen, X., Carpenter, B. M., & Reches, Z. E. (2020). Asperity failure control of stick–slip along brittle faults. *Pure and Applied Geophysics*, *177*(7), 3225–3242. https://doi.org/10.1007/s00024-020-02434-y

Chiarabba, C., De Gori, P., Latorre, D., & Amato, A. (2014). Crustal structure in the area of the 2002 Molise earthquake: Clues for the evolution of the southern Apennines. *Tectonics*, *33*(5), 1574–1594. https://doi.org/10.1002/2013tc003406

Chilovi, C., de Feyter, A. J., & Pompucci, A. (2000). Wrench zone reactivation in the Adriatic Block; the example of the Mattinata fault system (SE Italy). *Bollettini della Società Geologica Italiana*, *119*(1), 3–8.

Collettini, C., Niemeijer, A., Viti, C., & Marone, C. (2009). Fault zone fabric and fault weakness. *Nature*, *462*(7275), 907–910. https://doi.org/10.1038/nature08585

Coppola, M., Correale, A., Barberio, M. D., Billi, A., Cavallo, A., Fondriest, M., et al. (2021). Meso-to nano-scale evidence of fluid-assisted co-seismic slip along the normal mt. Morrone Fault, Italy: Implications for earthquake hydrogeochemical precursors. *Earth and Planetary Science Letters*, *568*, 117010. https://doi.org/10.1016/j.epsl.2021.117010

Cotecchia, V., & Canitano, A. (1954). *Sull'affioramento delle "Pietre Nere" al Lago di Lesina* (Vol. 73, pp. 3–18). Bollettini della Società Geologica Italiana.

Cremonini, G., Elmi, C., & Selli, R. (1971). *Note illustrative della carta geologica d'Italia, alla scala 1:100.000; Foglio 156 "San Marco in Lamis* (p. 69). Servizio Geologico d'Italia.

Crescenti, U., & Vighi, L. (1964). *Caratteristiche genesi e stratigrafia dei depositi bauxitici cretacici del Gargano e delle Murge* (Vol. 83, pp. 283–350). Bollettini della Società Geologica Italiana.

Curzi, M., Billi, A., Aldega, L., Baneschi, I., Boschi, C., Caracausi, A., et al. (2026). Earthquake dynamics sustained by seismic CO_2. *Nature Communications*, *17*(1), 2766. https://doi.org/10.1038/s41467-026-69174-w

Del Gaudio, V., Pierri, P., Frepoli, A., Calcagnile, G., Venisti, N., & Cimini, G. B. (2007). A critical revision of the seismicity of Northern Apulia (Adriatic microplate—Southern Italy) and implications for the identification of seismogenic structures. *Tectonophysics*, *436*(1–4), 9–35. https://doi.org/10.1016/j.tecto.2007.02.013

Delle Piane, C., Clennell, M. B., Keller, J. V., Giwelli, A., & Luzin, V. (2017). Carbonate hosted fault rocks: A review of structural and microstructural characteristic with implications for seismicity in the upper crust. *Journal of Structural Geology*, *103*, 17–36. https://doi.org/10.1016/j.jsg.2017.09.003

Del Viscio, G., Frijia, G., Posenato, R., Singh, P., Lehrmann, D. J., Payne, J. L., et al. (2021). Proliferation of Chondrodonta as a proxy of environmental instability at the onset of OAE1a: Insights from shallow-water limestones of the Apulia Carbonate Platform. *Sedimentology*, *68*(7), 3191–3227. https://doi.org/10.1111/sed.12887

Di Bucci, D., & Mazzoli, S. (2003). The October–November (2002) Molise seismic sequence (southern Italy): An expression of Adria intraplate deformation. *Journal of the Geological Society London*, *160*(4), 503–506. https://doi.org/10.1144/0016-764902-152

Di Bucci, D., Ravaglia, A., Seno, S., Toscani, G., Fracassi, U., & Valensise, G. (2006). Seismotectonics of the southern Apennines and Adriatic foreland: Insights on active regional E-W shear zones from analogue modeling. *Tectonics*, *25*(4), 1–21. https://doi.org/10.1029/2005TC001898

Di Toro, G., Han, R., Hirose, T., De Paola, N., Nielsen, S., Mizoguchi, K., et al. (2011). Fault lubrication during earthquakes. *Nature*, *471*(7339), 494–498. https://doi.org/10.1038/nature09838

Doglioni, C., Mongelli, F., & Pieri, P. (1994). The Puglia uplift (SE Italy): An anomaly in the foreland of the Apenninic subduction due to buckling of a thick continental lithosphere. *Tectonics*, *13*(5), 1309–1321. https://doi.org/10.1029/94TC01501

Faulkner, D. R., Lewis, A. C., & Rutter, E. H. (2003). On the internal structure and mechanics of large strike-slip fault zones: Field observations of the Carboneras fault in southeastern Spain. *Tectonophysics*, *367*(3–4), 235–251. https://doi.org/10.1016/S0040-1951(03)00134-3

Faulkner, D. R., Mitchell, T. M., Behnsen, J., Hirose, T., & Shimamoto, T. (2011). Stuck in the mud? Earthquake nucleation and propagation through accretionary forearcs. *Geophysical Research Letters*, *38*(18), L18303. https://doi.org/10.1029/2011GL048552

Ferreri, A. P., Romeo, A., Giannuzzi, R., Ninivaggi, T., Filippucci, M., Cecere, G., et al. (2025). The new seismic catalog of the Gargano area (Southern Italy) after a decade of seismic monitoring by OTRIONS network. *Earth System Science Data*, *2025*, 1–39. https://doi.org/10.5194/essd-2025-335

Filippucci, M., Miccolis, S., Castagnozzi, A., Cecere, G., de Lorenzo, S., Donvito, G., et al. (2021). Seismicity of the Gargano promontory (Southern Italy) after 7 years of local seismic network operation: Data release of waveforms from 2013 to 2018. *Data in Brief*, *35*, 106783. https://doi.org/10.1016/j.dib.2021.106783

Fracassi, U., Di Bucci, D., Ridente, D., Trincardi, F., & Valensise, G. (2012). Recasting historical earthquakes in coastal areas (Gargano Promontory, Italy): Insights from marine paleoseismology. *Bulletin of the Seismological Society of America*, *102*(1), 1–17. https://doi.org/10.1785/0120110001

Funiciello, R., Montone, P., Salvini, F., & Tozzi, M. (1988). Caratteri strutturali del Promontorio del Gargano. *Memorie della Societa Geologica Italiana*, *41*, 1235–1243.

Gu, D., Han, R., & Woo, S. (2021). Geological records of coseismic shear localization along the Yangsan fault, Korea. *Journal of Geophysical Research: Solid Earth*, *126*(8), e2020JB021393. https://doi.org/10.1029/2020JB021393

Hodgetts, D., Gawthorpe, R. L., Wilson, P., & Rarity, F. (2007). Integrating digital and traditional field techniques using virtual reality geological studio (VRGS) (Version 3.0.2) [Software]. In *69th EAGE Conference and exhibition incorporating SPE EUROPEC 2007* (pp. cp-27). European Association of Geoscientists and Engineers. https://doi.org/10.3997/2214-4609.201401718

Ikari, M. J., Saffer, D. M., & Marone, C. (2009). Frictional and hydrologic properties of clay-rich fault gouge. *Journal of Geophysical Research*, *114*(B5). https://doi.org/10.1029/2008JB006089

Kirkpatrick, J. D., Savage, H. M., Regalla, C., Shreedharan, S., Ross, C., Okuda, H., et al. (2025). Extreme plate boundary localization promotes shallowearthquake slip at the Japan Trench. *Science*, *391*(6784), 489–493. https://doi.org/10.1126/science.ady0234

Lin, A. (1996). Injection veins of crushing-originated pseudotachylyte and fault gouge formed during seismic faulting. *Engineering Geology*, *43*(2–3), 213–224. https://doi.org/10.1016/0013-7952(96)00062-2

Malinverno, A., & Ryan, W. B. (1986). Extension in the Tyrrhenian Sea and shortening in the Apennines as result of arc migration driven by sinking of the lithosphere. *Tectonics*, *5*(2), 227–245. https://doi.org/10.1029/TC005i002p00227

Martinis, B., & Pieri, M. (1964). Alcune notizie sulla formazione evaporitica del Triassico superiore nell'Italia centrale e meridionale. *Memorie della Società Geolgica Italiana*, *4*(1963), 649–678.

Miccolis, S., Filippucci, M., De Lorenzo, S., Frepoli, A., Pierri, P., & Tallarico, A. (2021). Seismogenic structure orientation and stress field of the Gargano Promontory (southern Italy) from microseismicity analysis. *Frontiers in Earth Science*, *9*, 589332. https://doi.org/10.3389/feart.2021.589332

21699356, 2026, 5, Downloaded from https://agupubs.onlinelibrary.wiley.com/doi/10.1029/2026JB033855 by Andrea Billi - University Di Roma La Sapienza , Wiley Online Library on [14/05/2026]. See the Terms and Conditions (https://onlinelibrary.wiley.com/terms-and-conditions) on Wiley Online Library for rules of use; OA articles are governed by the applicable Creative Commons License

Milano, G., Di Giovambattista, R., & Ventura, G. (2005). Seismic constraints on the present-day kinematics of the Gargano foreland, Italy, at the transition zone between the southern and northern Apennine belts. *Geophysical Research Letters*, *32*(24). https://doi.org/10.1029/2005GL024604

Moore, D. E., & Lockner, D. A. (2004). Crystallographic controls on the frictional behavior of dry and water-saturated sheet structure minerals. *Journal of Geophysical Research*, *109*(B3), B03401. https://doi.org/10.1029/2003JB002582

Morsilli, M. (2016). Sintesi delle conoscenze geologiche e stratigrafiche del Promontorio del Gargano. *Geologia e territorio*, *13*(2), 15–30.

Morsilli, M., & Bosellini, A. (1997). Carbonate facies zonation of the Upper Jurassic-Lower Cretaceous Apulia Platform Margin. *Rivista Italiana di Paleontologia e Stratigrafia*, *103*, 193–206.

Nicolai, C., & Gambini, R. (2007). Structural architecture of the Adria platform-and-basin system. *Bollettini della Società Geologica Italiana*, *7*, 21–37.

Otsuki, K., Uduki, T., Monzawa, N., & Tanaka, H. (2005). Clayey injection veins and pseudotachylyte from two boreholes penetrating the Chelungpu Fault, Taiwan: Their implications for the contrastive seismic slip behaviors during the 1999 chi-chi earthquake. *Island Arc*, *14*(1), 22–36. https://doi.org/10.1111/j.1440-1738.2004.00455.x

Patacca, E., & Scandone, P. (2004a). The Plio-Pleistocene thrust belt-foredeep system in the southern Apennines and Sicily (Italy). *Geology of Italy*, *32*, 93–129.

Patacca, E., & Scandone, P. (2004b). The 1627 Gargano earthquake (Southern Italy): Identification and characterization of the causative fault. *Journal of Seismology*, *8*(2), 259–273. https://doi.org/10.1023/B:JOSE.0000021393.77543.1e

Petricca, P., Carafa, M. M., Barba, S., & Carminati, E. (2013). Local, regional, and plate scale sources for the stress field in the Adriatic and periadriatic region. *Marine and Petroleum Geology*, *42*, 160–181. https://doi.org/10.1016/j.marpetgeo.2012.08.005

Rice, J. R. (2006). Heating and weakening of faults during earthquake slip. *Journal of Geophysical Research*, *111*(B5). https://doi.org/10.1029/2005JB004006

Rowe, C. D., & Griffith, W. A. (2015). Do faults preserve a record of seismic slip: A second opinion. *Journal of Structural Geology*, *78*, 1–26. https://doi.org/10.1016/j.jsg.2015.06.006

Ruggieri, R., Scuderi, M. M., Trippetta, F., Tinti, E., Brignoli, M., Mantica, S., et al. (2021). The role of shale content and pore-water saturation on frictional properties of simulated carbonate faults. *Tectonophysics*, *807*, 228811. https://doi.org/10.1016/j.tecto.2021.228811

Salvini, F., Billi, A., & Wise, D. U. (1999). Strike-slip fault-propagation cleavage in carbonate rocks: The Mattinata Fault Zone, Southern Apennines, Italy. *Journal of Structural Geology*, *21*(12), 1731–1749. https://doi.org/10.1016/S0191-8141(99)00120-0

Schleicher, A. M., & Jurado, M.-J. (2019). Linking faults, fractures, and clay mineral occurrence with fluid transport in the accretionary prism ofthe Nankai Trough, Japan. Geochemisty, Geophysics. *Geosystem*, *20*(11), 4599–4612. https://doi.org/10.1029/2019GC008430

Scholz, C. H. (1998). Earthquakes and friction laws. *Nature*, *391*(6662), 37–42. https://doi.org/10.1038/34097

Sibson, R. H. (1977). Fault rocks and fault mechanisms. *Journal of the Geological Society*, *133*(3), 191–213. https://doi.org/10.1144/gsjgs.133.3.0191

Siman-Tov, S., Aharonov, E., Sagy, A., & Emmanuel, S. (2013). Nanograins form carbonate fault mirrors. *Geology*, *41*(6), 703–706. https://doi.org/10.1130/G34087.1

Smeraglia, L., Aldega, L., Billi, A., Carminati, E., & Doglioni, C. (2016). Phyllosilicate injection along extensional carbonate-hosted faults and implications for co-seismic slip propagation: Case studies from the central Apennines, Italy. *Journal of Structural Geology*, *93*, 29–50. https://doi.org/10.1016/j.jsg.2016.10.003

Smeraglia, L., Bettucci, A., Billi, A., Carminati, E., Cavallo, A., Di Toro, G., et al. (2017). Microstructural evidence for seismic and aseismic slips along clay-bearing, carbonate faults. *Journal of Geophysical Research: Solid Earth*, *122*(5), 3895–3915. https://doi.org/10.1002/2017JB014042

Smeraglia, L., Billi, A., Carminati, E., Cavallo, A., Di Toro, G., Spagnuolo, E., & Zorzi, F. (2017). Ultra-thin clay layers facilitate seismic slip in carbonate faults. *Scientific Reports*, *7*(1), 664. https://doi.org/10.1038/s41598-017-00717-4

Smith, S. A., Billi, A., Toro, G. D., & Spiess, R. (2011). Principal slip zones in limestone: Microstructural characterization and implications for the seismic cycle (Tre Monti Fault, Central Apennines, Italy). *Pure and Applied Geophysics*, *168*(12), 2365–2393. https://doi.org/10.1007/s00024-011-0267-5

Tesei, T., Collettini, C., Viti, C., & Barchi, M. R. (2013). Fault architecture and deformation mechanisms in exhumed analogues of seismogenic carbonate-bearing thrusts. *Journal of Structural Geology*, *55*, 167–181. https://doi.org/10.1016/j.jsg.2013.07.007

Tinti, S., Maramai, A., & Favali, P. (1995). The Gargano promontory: An important Italian seismogenic–tsunamigenic area. *Marine Geology*, *122*(3), 227–241. https://doi.org/10.1016/0025-3227(94)00096-4

Tinti, S., & Piatanesi, A. (1996). Numerical simulations of the tsunami induced by the 1627 earthquake affecting Gargano, southern Italy. *Journal of Geodynamics*, *21*(2), 141–160. https://doi.org/10.1016/0264-3707(95)00021-4

Tondi, E., Piccardi, L., Cacon, S., Kontny, B., & Cello, G. (2005). Structural and time constraints for dextral shear along the seismogenic Mattinata Fault (Gargano, southern Italy). *Juornal of Geodynamics*, *40*(2–3), 134–152. https://doi.org/10.1016/j.jog.2005.07.003

Trippetta, F., Petricca, P., Billi, A., Collettini, C., Cuffaro, M., Lombardi, A. M., et al. (2019). From mapped faults to fault-length earthquake magnitude (FLEM): A test on Italy with methodological implications. *Solid Earth*, *10*(5), 1555–1579. https://doi.org/10.5194/se-10-1555-2019

Uysal, I. T., Feng, Y. X., Zhao, J. X., Bolhar, R., Işik, V., Baublys, K. A., et al. (2011). Seismic cycles recorded in late Quaternary calcite veins: Geochronological, geochemical and microstructural evidence. *Earth and Planetary Science Letters*, *303*(1–2), 84–96. https://doi.org/10.1016/j.epsl.2010.12.039

Vallée, M., & Di Luccio, F. (2005). Source analysis of the 2002 Molise, southern Italy, twin earthquakes (10/31 and 11/01). *Geophysical Research Letters*, *32*(12), L12309. https://doi.org/10.1029/2005GL022687

Vannucchi, P., Remitti, F., & Bettelli, G. (2008). Geological record of fluid flow and seismogenesis along an erosive subducting plate boundary. *Nature*, *451*(7179), 699–703. https://doi.org/10.1038/nature06486

Vezzani, L., Festa, A., & Ghisetti, F. C. (2010). Geology and tectonic evolution of the Central-Southern Apennines, Italy. *Geological Society of America Bulletin*, *469*. https://doi.org/10.1130/2010.2469

Vingiani, S., Di Iorio, E., Colombo, C., & Terribile, F. (2018). Integrated study of red Mediterranean soils from southern Italy. *Catena*, *168*, 129–140. https://doi.org/10.1016/j.catena.2018.01.002

Violay, M., Nielsen, S., Spagnuolo, E., Cinti, D., Di Toro, G., & Di Stefano, G. (2013). Pore fluid in experimental calcite-bearing faults: Abrupt weakening and geochemical signature of co-seismic processes. *Earth and Planetary Science Letters*, *361*, 74–84. https://doi.org/10.1016/j.epsl.2012.11.021

Viti, C., & Collettini, C. (2009). Growth and deformation mechanisms of talc along a natural fault: A micro/nanostructural investigation. *Contributions to Mineralogy and Petrology*, *158*(4), 529–542. https://doi.org/10.1007/s00410-009-0395-4

21699356, 2026, 5, Downloaded from https://agupubs.onlinelibrary.wiley.com/doi/10.1029/2026JB033855 by Andrea Billi - University Di Roma La Sapienza , Wiley Online Library on [14/05/2026]. See the Terms and Conditions (https://onlinelibrary.wiley.com/terms-and-conditions) on Wiley Online Library for rules of use; OA articles are governed by the applicable Creative Commons License

References From the Supporting Information

Moore, D. M., & Reynolds, R. C. Jr., (1997). *X-Ray Diffraction and the identification and analysis of clay minerals*. Oxford University Press, 378. https://doi.org/10.1017/S0016756898501501

Whitney, D. L., & Evans, B. W. (2010). Abbreviations for names of rock-forming minerals. *American Mineralogist*, *95*(1), 185–187. https://doi.org/10.2138/am.2010.3371

21699356, 2026, 5, Downloaded from https://agupubs.onlinelibrary.wiley.com/doi/10.1029/2026JB033855 by Andrea Billi - University Di Roma La Sapienza , Wiley Online Library on [14/05/2026]. See the Terms and Conditions (https://onlinelibrary.wiley.com/terms-and-conditions) on Wiley Online Library for rules of use; OA articles are governed by the applicable Creative Commons License